Supporting Information: Allosteric DNAzyme-based DNA logic Circuit: Operations and Dynamic Analysis

Xuedong Zheng[1], Jing Yang[4], Changjun Zhou[5], Cheng Zhang[6,*], Qiang Zhang[2,3*], and Xiaopeng Wei[2,3*]

[1] College of Computer Science, Shenyang Aerospace University, Shenyang 110136, China.

[2] School of Computer Science and Technology, Dalian University of Technology, Dalian 116024, China.

[3] Key Laboratory of Advanced Design and Intelligent Computing, Dalian University, Ministry of Education, Dalian 116622, China

[4] School of Control and Computer Engineering, North China Electric Power University, Beijing 102206, China.

[5] College of Mathematics and Computer sciences, Zhejiang Normal University, Jinhua, 321004, China.

[6] School of Electronics Engineering and Computer Science, Peking University, Key laboratory of High Confidence Software Technologies, Ministry of Education, Beijing 100871, China

* To whom correspondence should be addressed. Email: zhangq@dlut.edu.cn. Correspondence may also be addressed to Cheng Zhang, email: zhangcheng369@pku.edu.cn, and Xiaopeng Wei, email: xpwei@dlut.edu.cn.

Table of Contents

S1: Allosteric regulation of DNAzyme

S1.1: DNAzyme cleavage

As a pre-experiment, DNAzyme digestion was firstly testified to ensure DNAzyme to cleave its substrate correctly. Figure S1 shows the possible reactions of DNAzyme digestion in this study. The reaction of DNAzyme digestion includes two kinds of processes, one is the direct cleavage of substrate (Figure S1A), and the other is the cleavage induced by DNAzyme displacement (1-4) (Figure S1B).
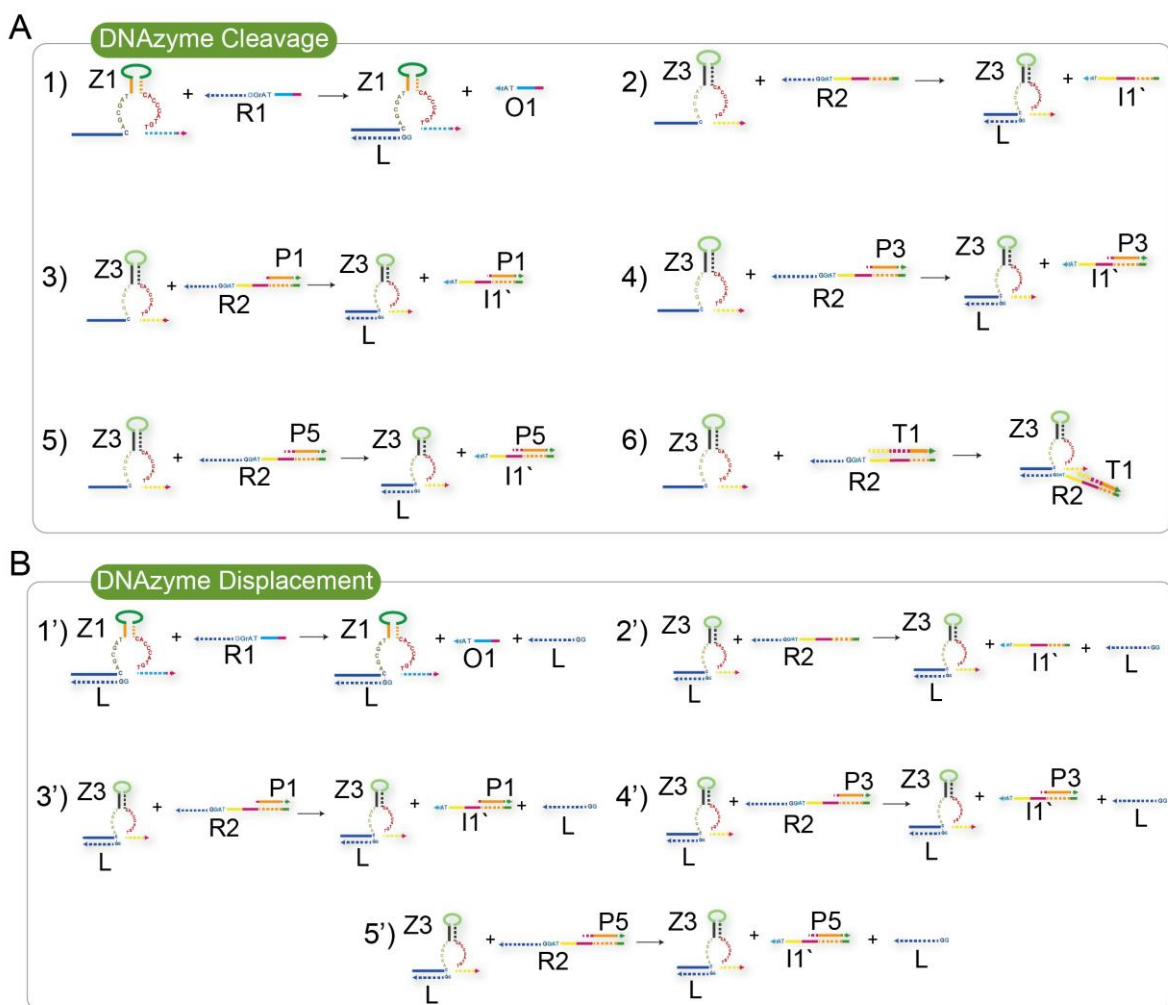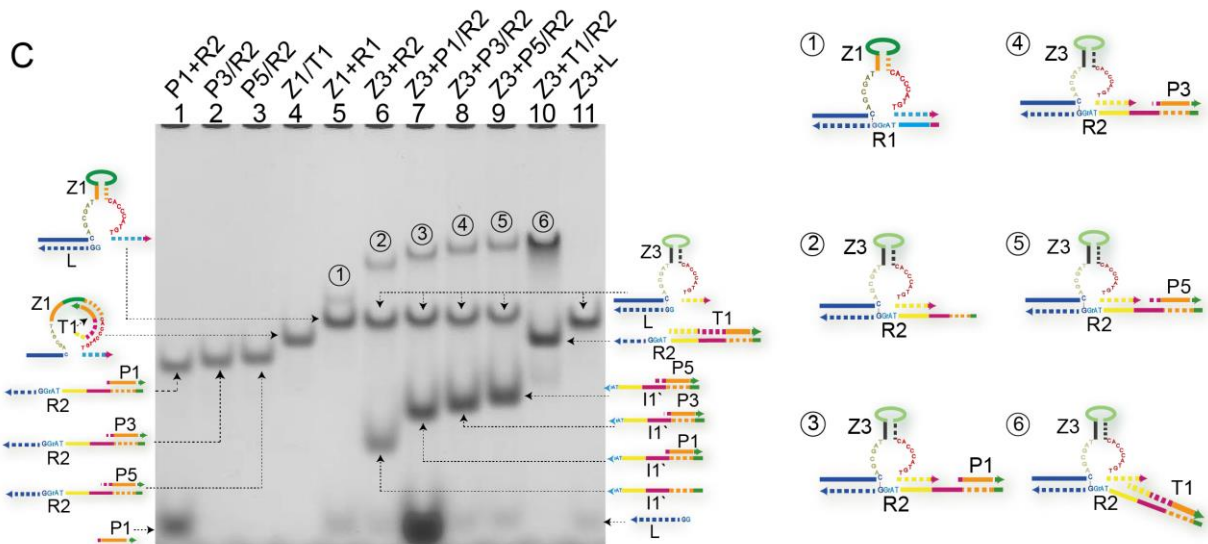
Figure S1. (A) Illustration of direct DNAzyme digestion. (B) Illustration of possible DNAzyme cleavage induced by DNAzyme displacement. (C) Native PAGE analysis of DNAzyme-cleavage products. Lane 1, substrate P1/R2 and protector P1; lane 2, substrate P3/R2; lane 3, substrate P5/R2; lane 4, DNAzyme complex Z1/T1; lane 5, products of DNAzyme Z1 cleaving substrate R1 ([Z1]:[R1]=1:3); lane 6, products of DNAzyme Z3 cleaving substrate R2 ([Z3]:[R2]=1:3); lane 7, products of DNAzyme Z3 cleaving substrate P1/R2 ([Z3]:[P1/R2]=1:3); lane 8, products of DNAzyme Z3 cleaving substrate P3/R2 ([Z3]:[P3/R2]=1:3); lane 9, products of DNAzyme Z3 cleaving substrate P5/R2 ([Z3]:[P5/R2]=1:3); lane 10, products of DNAzyme Z3 mixed with substrate T1/R2 ([Z3]:[T1/R2]=1:3); lane 11, DNAzyme complex Z3/L and strand L.

From Figure S1C, DNAzymes can cut the substrates with or without protectors (lanes 5-9). But DNAzyme Z3 cannot cut substrate T1/R2 (lane 10) because of not complete hybridization with its substrate. In addition, it can be concluded that DNAzyme displacement happened (lanes 5-9) because the gel band corresponding to the substrates disappeared. Another fact is that although the protectors P1, P3 and P5 existed, the DNAzyme displacement still happened (lanes 7-9).

S1.2: DNAzyme displacement

Inspired by the results in Figure S1, further experiments (Figure S2 and Figure S3) were done to test DNAzyme displacement with DNA or RNA-modified substrate, where the toehold length of substrate was slightly shorter than that of substrate-binding arm of DNAzyme.
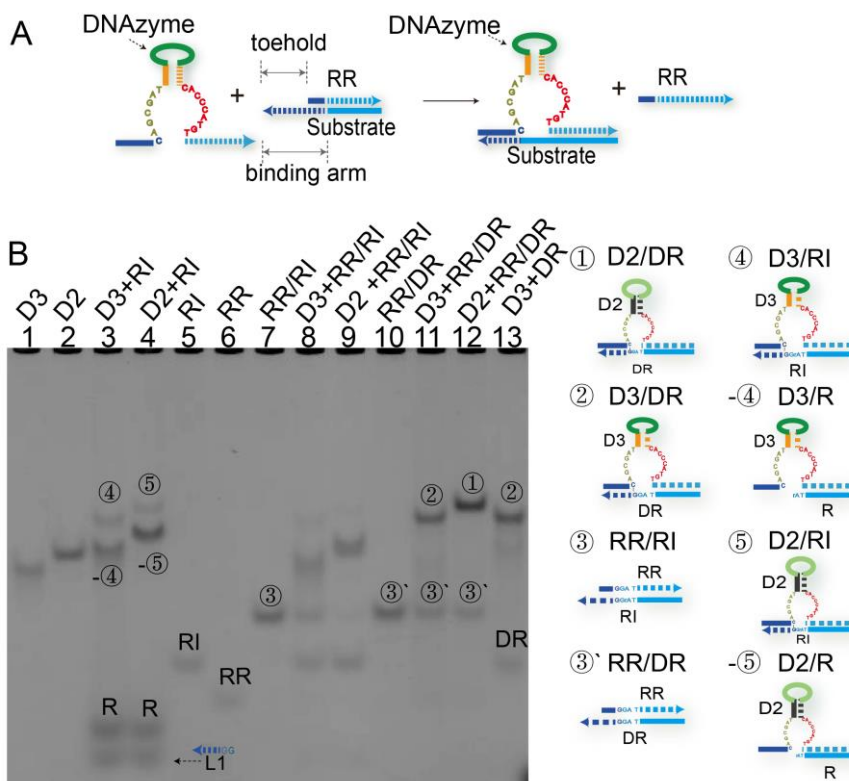
Figure S2. (A) Illustration of DNAzyme displacement where toehold located at 3' end of substrate. (B) Native PAGE analysis of DNAzyme-displacement products. Strands D2 and D3 are DNAzymes, strand RI is the RNA-modified substrate and strand DR is the corresponding DNA substrate. Lane 1, DNAzyme D3; lane 2, DNAzyme D2; lane 3, products of DNAzyme D3 cleaving RNA-modified substrate RI ([D3]:[RI]=1:3); lane 4, products of DNAzyme D2 cleaving RNA-modified substrate RI ([D2]:[RI]=1:3); lane 5, RNA-modified substrate RI; lane 6, strand RR; lane 7, duplex RR/RI; lane 8, products of DNAzyme D3 mixed with RNA modified substrate RR/RI ([D3]:[RR/RI]=1:1); lane 9, products of DNAzyme D2 mixed with RNA modified substrate RR/RI ([D2]:[RR/RI]=1:1); lane 10, duplex RR/DR; lane 11, products of DNAzyme D3 mixed with DNA substrate RR/DR ([D3]:[RR/DR]=1:1.5); lane 12, products of DNAzyme D2 mixed with DNA substrate RR/DR ([D2]:[RR/DR]=1:1.5); lane 13, products of DNAzyme complex D3 mixed with DNA substrate DR ([D3]:[DR]=1:2).

According to Figure S2B, DNAzymes D3 and D2 can cut the RNA-modified substrate RI accompanying with DNAzyme displacement (lanes 3 and 4). However, when RI hybridized with its partially complementary strand RR, the DNAzyme cleavage and displacement (lanes 8 and 9) were not as clear as happened in lanes 3 and 4. But interestingly, when the substrate was replaced by DNA strand with the same bases, DNAzyme displacement

happened (lanes 11 and 12) although the 'cleavage site' of substrate DR was covered by strand RR.
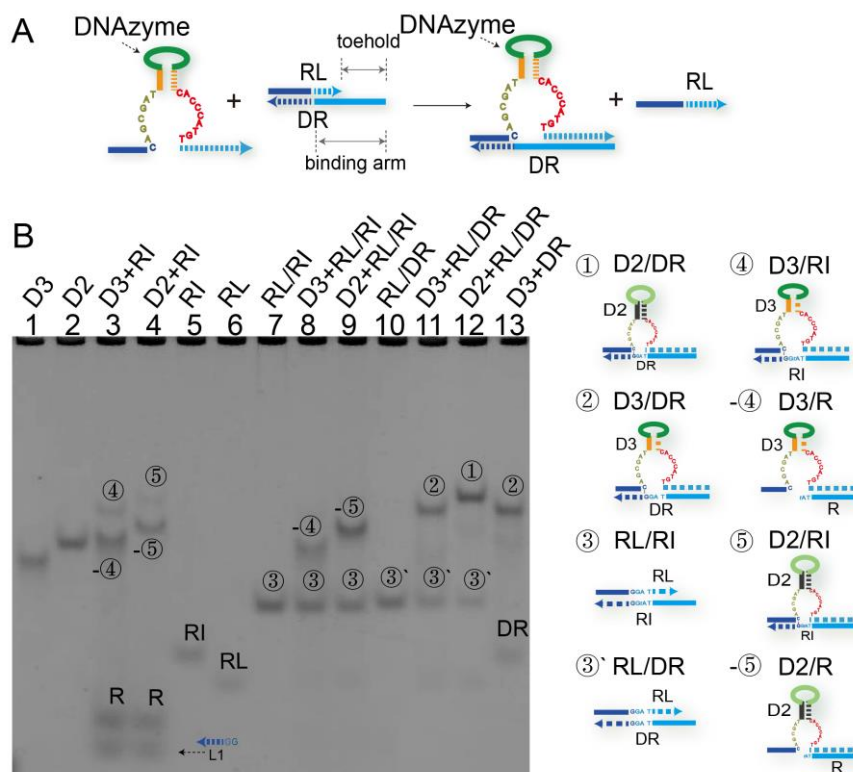

Figure S3. (A) Illustration of DNAzyme displacement where toehold located at 5' end of substrate. (B) Native PAGE analysis of DNAzyme-displacement products. Lane 1, DNAzyme D3; lane 2, DNAzyme D2; lane 3, products of DNAzyme D3 cleaving RNA-modified substrate RI ([D3]:[RI]=1:3); lane 4, products of DNAzyme D2 cleaving RNA-modified substrate RI ([D2]:[RI]=1:3); lane 5, RNA-modified substrate RI; lane 6, strand RL; lane 7, duplex RL/RI; lane 8, products of DNAzyme D3 mixed with RNA-modified substrate RL/RI ([D3]:[RL/RI]=1:1); lane 9, products of DNAzyme D2 mixed with RNA modified substrate RL/RI ([D2]:[RR/RI]=1:1); lane 10, duplex RL/DR; lane 11, products of DNAzyme D3 mixed with DNA substrate RL/DR ([D3]:[RL/DR]=1:1.5); lane 12, products of DNAzyme D2 mixed with DNA substrate RL/DR ([D2]:[RL/DR]=1:1.5); lane 13, products of DNAzyme complex D3 mixed with DNA substrate DR ([D3]:[DR]=1:2).

From Figure S3B, DNAzyme displacement happened in the case of DNA substrate (lanes 11 and 12). But different from the corresponding cases in Figure S2B, there were some DNAzyme displacement happened in lanes 8 and 9.

From the experimental results in Figure S2 and S3, in the case of DNA substrate, DNAzyme can be used to implement some remote displacement (5) in the presence of

magnesium ion, and the substrate-binding arm of DNAzyme can be viewed as a single DNA strand logically to perform strand displacement.

S1.3: Optimization for logic unit

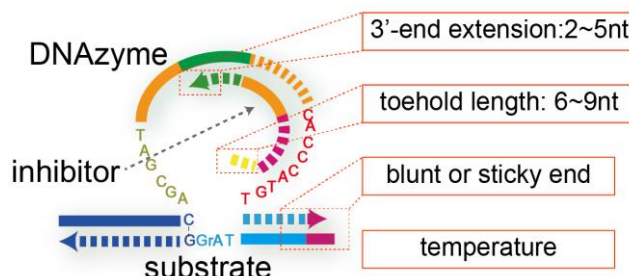Control experiments were done to optimize the formation of logic unit.

Figure S4. Optimizing factors of logic unit.

As shown in Figure S4, temperature, 3'-end extension of inhibitor, toehold length of inhibitor and style of substrate-binding end were selected as four optimizing factors. The control experimental results are shown in Figure S5 and S6.
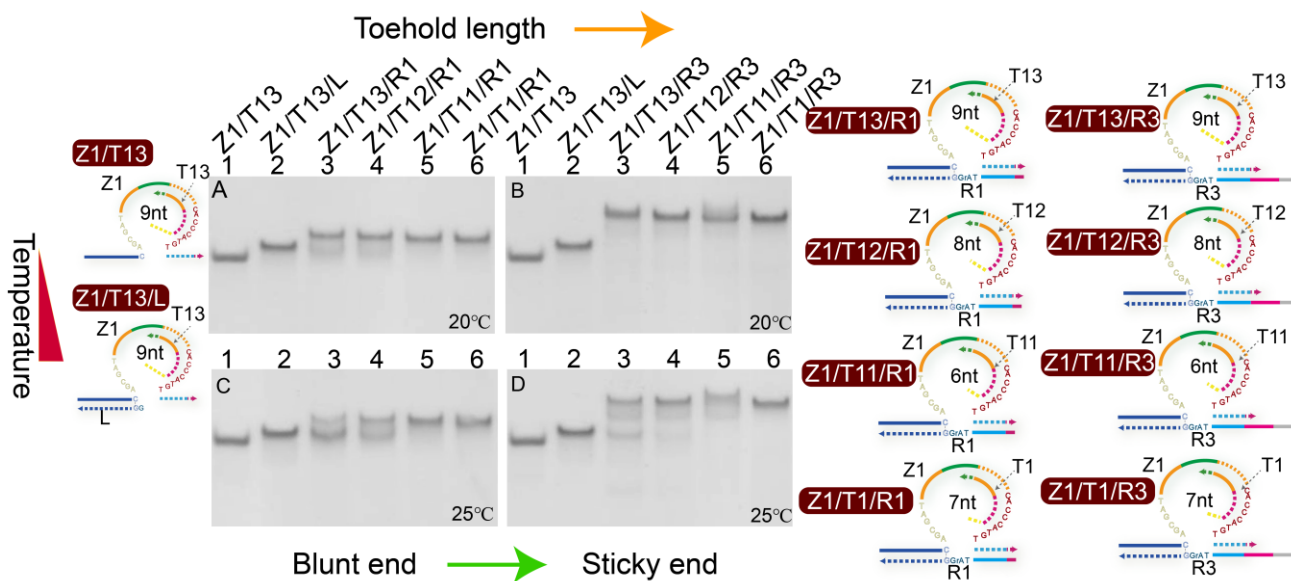

Figure S5. Native PAGE analysis of the impacts of temperature, toehold length of inhibitor and style of substrate-binding end. The logic unit was prepared by annealing twice: firstly, the mixture of inhibitor strands and DNAzymes in 1×TAE/Mg2+ buffer was annealed and preserved at 20°C (subfigure A and B) or 25°C (subfigure C and D); and then the substrates were added into the annealed mixture and incubated at constant temperature 20°C (subfigure A and B) or 25°C (subfigure C and D) for 4 hours. The toehold length of inhibitor was labeled in graphic symbols. Lane 1, DNAzyme complex Z1/T13; lane 2

DNAzyme complex Z1/T13/L. Lanes 3-6, logic units consisting of inhibitors with different toehold length.

From Figure S5, the toehold length of inhibitor has significant impact on the formation of logic unit (lanes 3-6). The impact is possibly attributed to the dangling of toehold which can hinder the substrate from binding DNAzyme. However, the style of substrate-binding end has little impact. In addition, the logic unit at 20℃ is more stable than that at 25℃. According to the results in Figure S5, the inhibitor T1 (lanes 6) shows good adaptability and is selected.
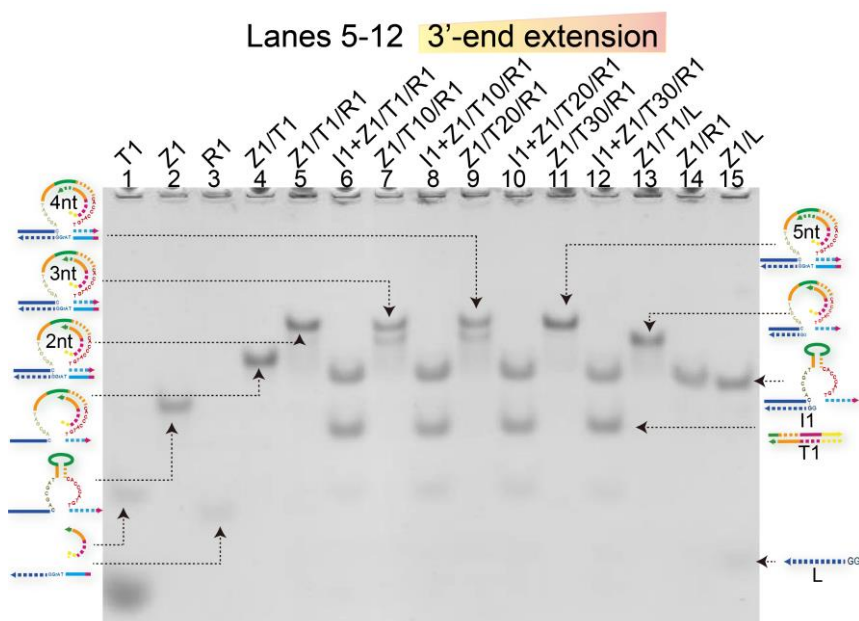

Figure S6. Native PAGE analysis of the impacts of 3'-end extension of inhibitor. Relative to the strand T1, the length of 3'-end extension of inhibitor at its 3' end was labeled in graphic symbols. Lanes 1-3, ssDNA as the elements of logic unit. Lane 4, DNAzyme Z1 hybridized with inhibitor T1; lanes 5, 7, 9 and 11, logic unit complex consisting of inhibitors with different 3'-end extension; lane 6, 8, 10 and 12, products of logic unit complex triggered by input I1; lane 13, DNAzyme complex Z1/T1/L; lane 14, products of DNAzyme Z1 cleaving substrate R1 ([Z1]:[R1]=1:1); lane 15, products of DNAzyme Z1 mixed with strand L ([Z1]:[L]=1:2).

From Figure S6, the extension of inhibitor at its 3' end has some symmetric impacts on the formation of logic unit (lanes 5, 7, 9 and 11), although the four logic units can make right response to the input I1 (lanes 6, 8, 10 and 12). But interestingly, the gel bands in lanes 5 and 11 has almost the same appearance and almost the same symmetric patterns can be found in lanes 7 and 9. These facts can be due to the symmetric configuration of hairpin

structure of DNAzyme.

S2: Development of DNA-based logic circuit

S2.1: YES gate

Figure S7A shows a generalized version of YES gate with sticky end to better use its released segment O3 to regulate downstream operation.
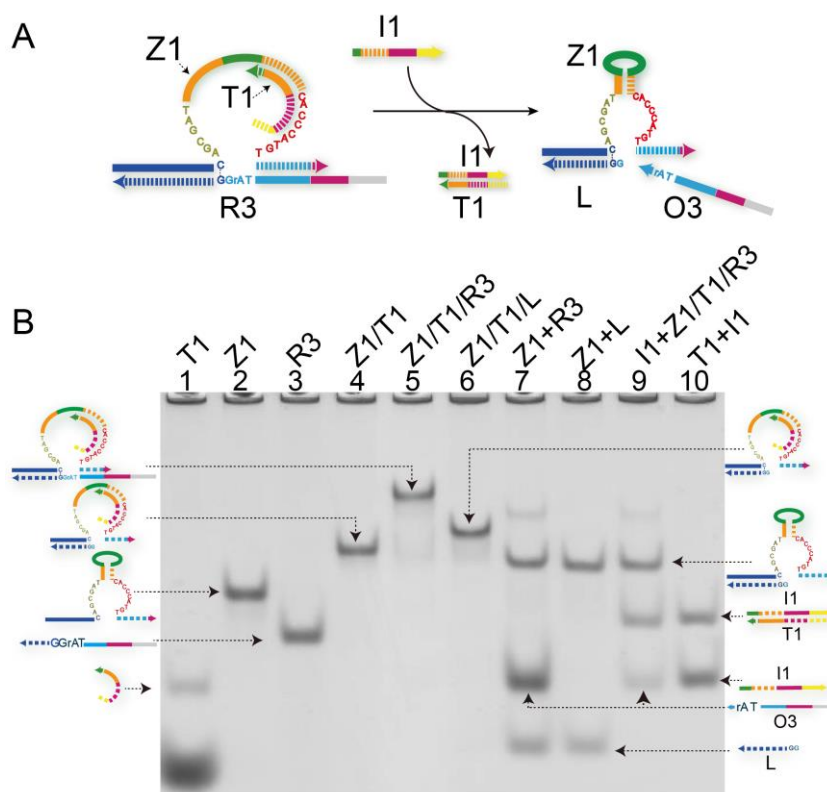

Figure S7. (A) Illustration of reaction. (B) Native PAGE analysis of reaction products. Lanes 1-3, ssDNA as the elements of the YES gate; lane 4, DNAzyme Z1 hybridized with inhibitor T1; lane 5, YES gate complex Z1/T1/R3; lane 6, DNAzyme complex Z1/T1/L; lane 7, products of DNAzyme digestion ([Z1]:[R3]=1:3); lane 8, products of DNAzyme Z1 mixed with strand L ([Z1]:[L]=1:3); lane 9; products of YES gate triggered by input I1; lane 10, products of inhibitor T1 mixed with input I1 ([T1]:[I1]=1:3).

From Figure S7B, the formation of YES gate complex with sticky end can be clearly observed in lane 5. And in the presence of input I1, the DNAzyme Z1 was activated and cut the substrate R3 (lane 9). After cleavage, the longer segment O3 was released and could be used to regulate downstream logic operation.

S2.2: OR gate

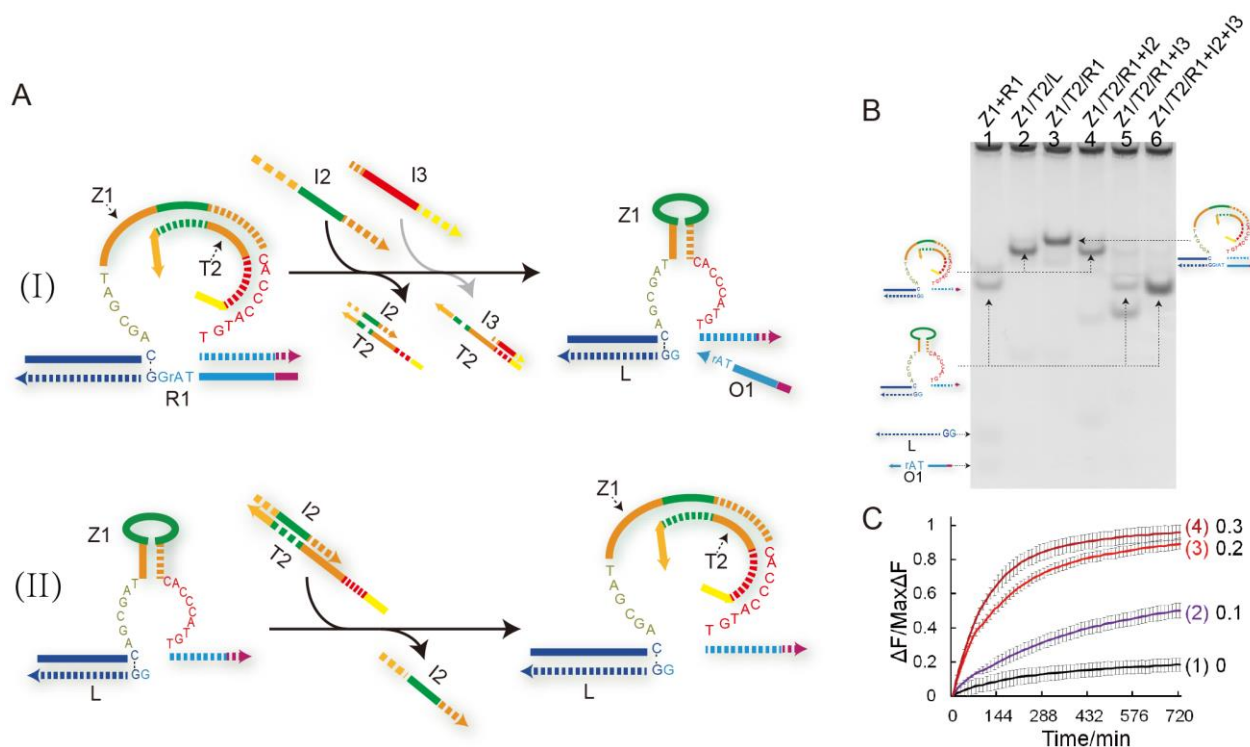Figure S8 presents the gel results as illustrated in Figure 2A.

Figure S8. (A) Illustration of OR operation. (B) Native PAGE analysis of OR-gate products. Lane 1, products of DNAzyme digestion ([Z1]:[R1]=1:3); lane 2, DNAzyme complex Z1/T2/L; lane 3, OR gate complex Z1/T2/R1; lane 4, products of OR logic operation triggered by input I2; lane 5, products of OR logic operation triggered by input I3; lane 6, products of OR logic operation triggered by both inputs I2 and I3. (C) Time-dependent normalized fluorescence changes (ΔF/MaxΔF) at different levels of input concentrations of I2. The sample interval was 6 minutes. Curves (1) to (4) demonstrate the gate responses at different concentrations of I2 as 0μM, 0.1μM, 0.2μM and 0.3μM, respectively. All data represent the average of three replicates. Error bars represent one standard deviation from triplicate analyses.

From PAGE gel experiment results (Figure S8B), the initial gel band corresponding to the OR gate complex (lane 3) disappeared in the presence of any one of input strand I2 or I3 (lanes 4 and 5), thus demonstrating the activation of DNAzyme. Similarly, when adding both of input strands I2 and I3, the active DNAzyme Z1 was also produced to trigger the cleavages of substrate R1 (lane 6). But as shown in lanes 4 and 5, although DNAzyme Z1 could be activated by input I2 or I3 properly, the response mechanisms of the OR gate were

11

different. Different from the trigger caused by single input I3 (reaction I in Figure S8A), another further strand displacement happened (reaction II in Figure S8B) in the presence of single input strand I2 and the input stand I2 was released after reaction II. The fact demonstrated that the input strand I2 played a role as a catalyst, thus indicating that low concentration of input strand I2 could activate DNAzyme Z1 (Figure S8C). Notably, when the concentration of input I2 was 0.1 µM (curve 2 in Figure S8C), the OR gate could also make proper response although approximate equal amount of free inhibitor T2 existed (where the molar ration in preparation of the OR gate was [Z1]:[T2]:[R1]=0.5:0.6:05). So, only in respect of the allosteric regulation of DNAzyme Z1, the OR gate triggered by single input I2 shows the feasibility to regulate the activation of DNAzyme Z1 reversibly without any cost of another fuel strands.

To make consistent behaviors of OR gate for different single input, in other words, to avoid reaction II in Figure S8A, further experiments were done as shown in Figure S9.
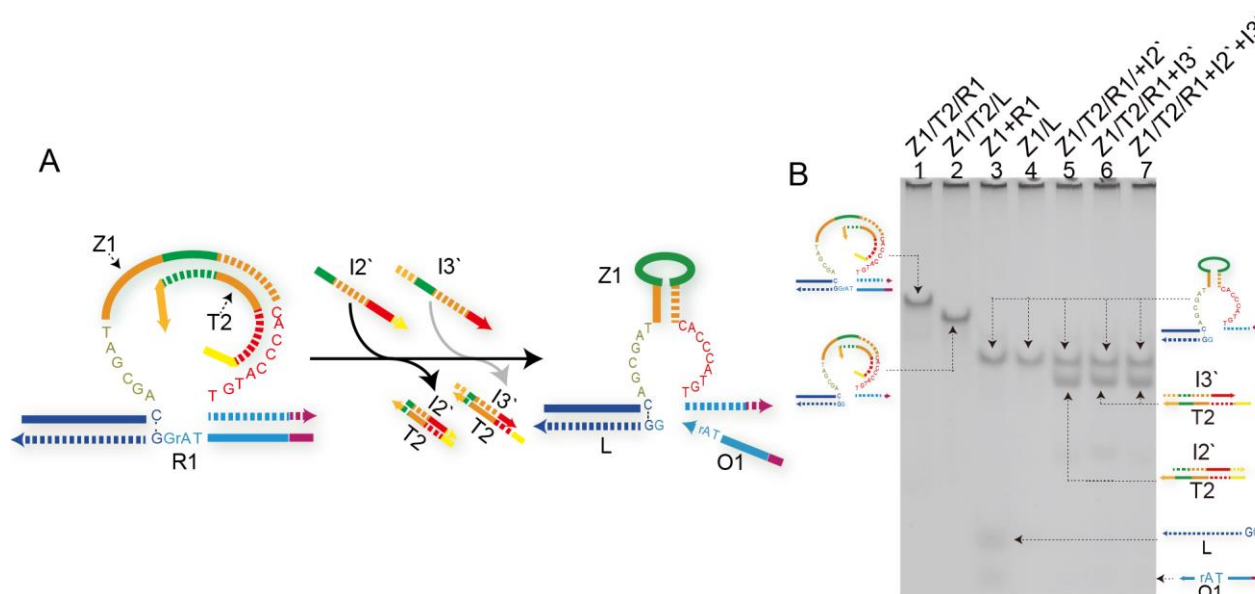

Figure S9. (A) Illustration of OR operation. (B) Native PAGE analysis of OR-gate products. Lane 1, OR gate complex Z1/T2/R1; lane 2, DNAzyme complex Z1/T2/L; lane 3, products of DNAzyme digestion ([Z1]:[R1]=1:3); lane 4, DNAzyme complex Z1/L; lane 5, products of OR logic operation triggered by input I2`; lane 6, products of OR logic operation triggered by input I3`; lane 7, products of OR logic operation triggered by both inputs I2` and I3`.

From PAGE gel experiment results (Figure S9B), the initial gel band corresponding to the OR gate complex (lane 1) disappeared in the presence of any one of input strand I2` or

I3` (lanes 5 and 6), thus demonstrating the activation of DNAzyme. Similarly, when adding both of input strands I2` and I3`, the active DNAzyme Z1 was also produced to trigger the cleavages of substrate R1 (lane 7). In addition, from the gel band shifts in lanes 5 and 6, the OR gate responded to single input I2` or I3` in a consistent way.

As a useful supplement, corresponding to the design of OR gate in Figure S9A, Figure S10 shows the version of OR gate with sticky end.
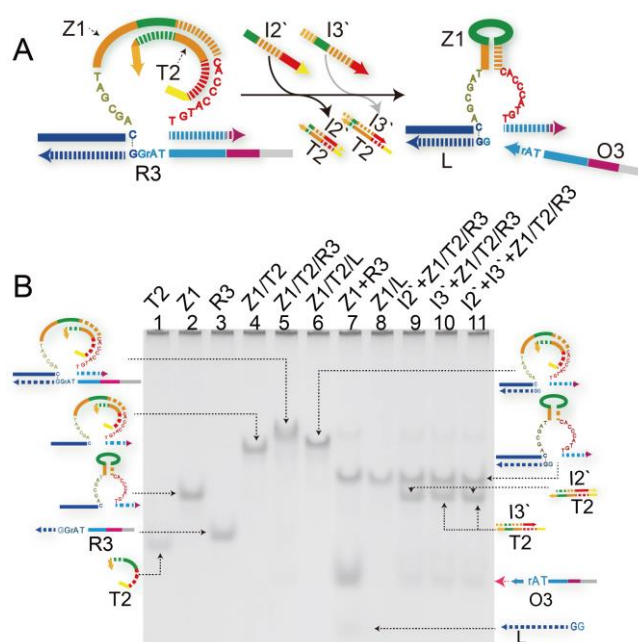

Figure S10. OR gate with sticky end. (A) Illustration of reaction. (B) Native PAGE analysis of reaction products. Lanes 1-3, ssDNA as the elements of the OR gate; lane 4, DNAzyme Z1 hybridized with inhibitor T2; lane 5, gate complex Z1/T2/R3; lane 6, DNAzyme complex Z1/T2/L; lane 7, products of DNAzyme digestion ([Z1]:[R3]=1:3); lane 8, DNAzyme complex Z1/L; lanes 9-11, products of OR operation triggered by one or two inputs, respectively.

The allosteric regulation of DNAzyme could not only be mediated by linear DNA but also the nonlinear DNA with some secondary structure. Figure S11A and S12A shows the design scheme of an OR gate in which the DNAzyme is regulated by the input strand with hairpin structure. In this scheme, the allosteric regulation is driven by the toehold located at the loop domain of DNAzyme Z5.
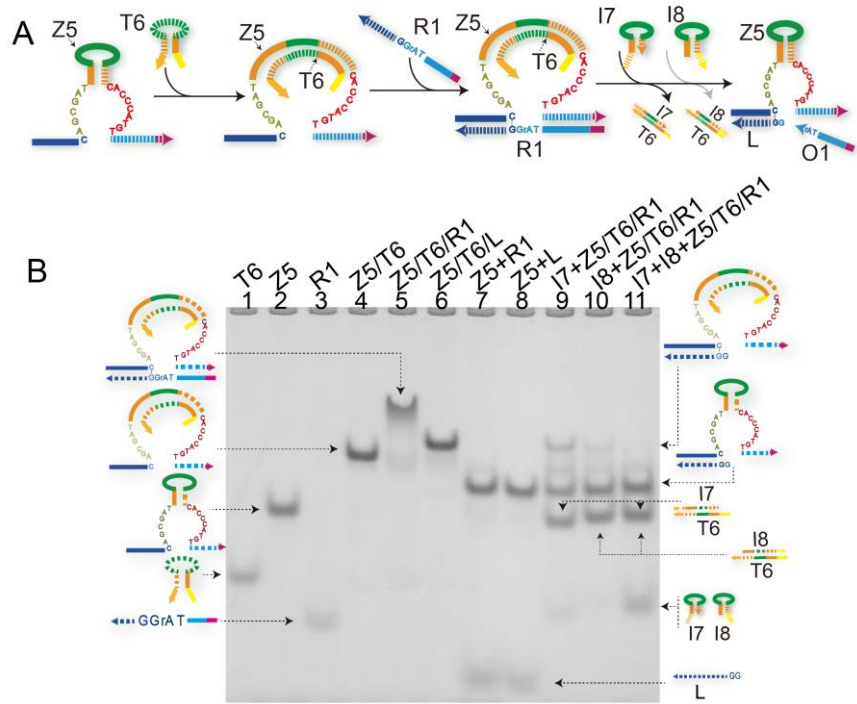
Figure S11. OR gate inhibited by hairpin strand with blunt end. (A) Illustration of reaction. (B) Native PAGE analysis of reaction products. Lanes 1-3, ssDNA as the elements of the OR gate; lane 4, DNAzyme Z5 hybridized with inhibitor T6; lane 5, gate complex Z5/T6/R1; lane 6, DNAzyme complex Z5/T6/L; lane 7, products of DNAzyme digestion ([Z5]:[R1]=1:3); lane 8, products of DNAzyme Z5 mixed with strand L ([Z5]:[L]=1:3); lanes 9, products of OR operation triggered by input I7; lane 10, products of OR operation triggered by input I8; lane 11, products of OR operation triggered by both inputs I7 and I8.

From Figure S11B, the OR gate complex can be observed in lane 5 and can be activated by strand I7 and I8 properly (lanes 9-11).

Figure S12 presents the corresponding version of the OR gate inhibited by hairpin strand with sticky end.
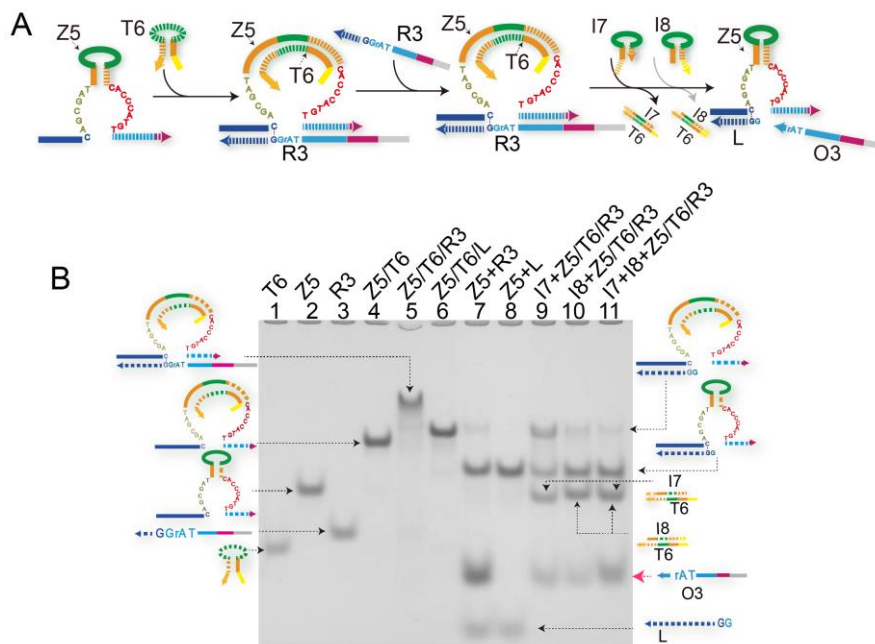
Figure S12. OR gate inhibited by hairpin strand with sticky end. (A) Illustration of reaction. (B) Native PAGE analysis of reaction products. Lanes 1-3, ssDNA as the elements of the OR gate; lane 4, DNAzyme Z5 hybridized with inhibitor T6; lane 5, gate complex Z5/T6/R3; lane 6, DNAzyme complex Z5/T6/L; lane 7, products of DNAzyme digestion ([Z5]:[R3]=1:3); lane 8, products of DNAzyme Z5 mixed with strand L ([Z5]:[L]=1:3); lanes 9, products of OR operation triggered by input I7; lane 10, products of OR operation triggered by input I8; lane 11, products of OR operation triggered by both inputs I7 and I8.

S2.3: AND gate

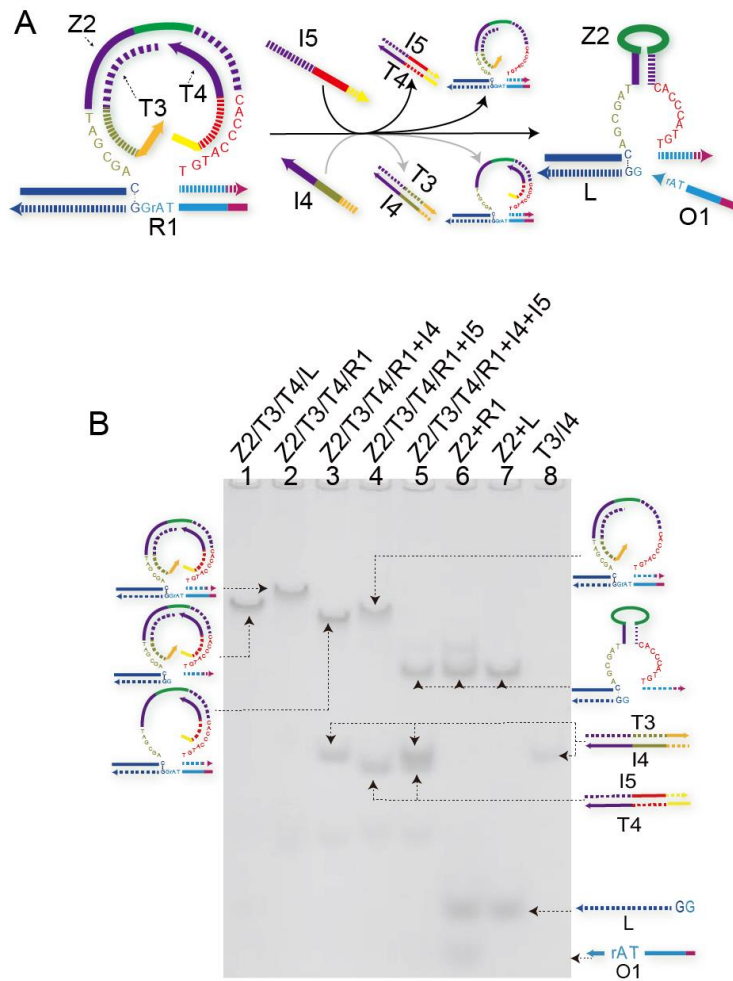Figure S13 presents the gel results as illustrated in Figure 2C.

Figure S13. (A) Illustration of AND operation. (B) Native PAGE analysis of AND-gate products. Lane 1, DNAzyme complex Z2/T3/T4/L; lane 2, gate complex Z2/T3/T4/R1; lane 3, products of AND operation triggered by single input I4; lane 4, products of AND operation triggered by single input I5; lane 5, products of AND operation triggered by both inputs I4 and I5; lane 6, products of DNAzyme digestion ([Z2]:[R1]=1:3); lane 7, products of DNAzyme Z2 mixed with strand L([Z2]:[L]=1:3); lane 8, duplex T3/I4.

As shown in Figure S13, the generation of the activation of DNAzyme Z2 can only be observed when treating with both strands I4 and I5 at the same time (lane 5), while additions of any one of them cannot lead to the generation of DNAzyme (lanes 3 and 4).

As illustrated in Figure S14A, DNAzyme Z2 was mutated to DNAzyme Z6. By using Z6 to develop a variant AND gate, the impact of hairpin domain of DNAzyme on the formation of AND gate was tested (Figure S14B and S14C).
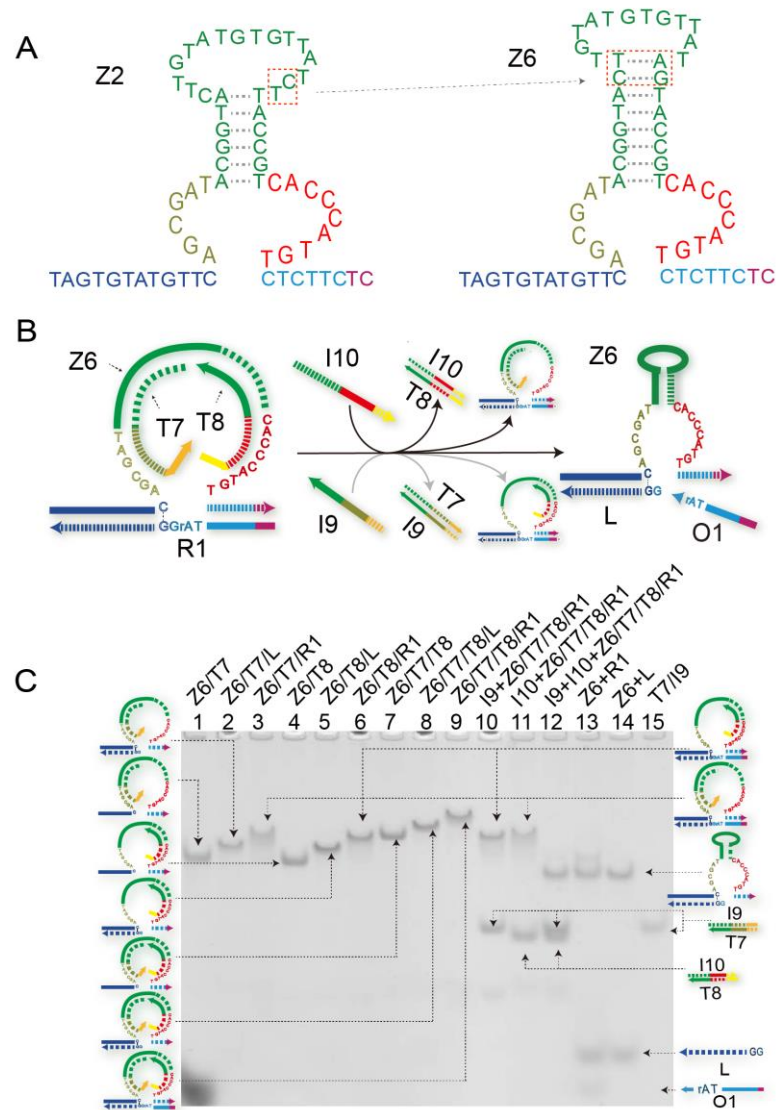
Figure S14. (A) Mutation of DNAzyme Z2→Z6. (B) Illustration of reaction. (C) Native PAGE analysis of reaction products. Lanes 1-8, different immediate products in the development of AND gate; lane 9, gate complex Z6/T7/T8/R1; lane 10-12, products of AND operation triggered by one or two inputs; lane 13, products of DNAzyme digestion ([Z6]:[R1]=1:3); lane 14, products of DNAzyme Z6 mixed with strand L ([Z6]:[L]=1:3); lane 15, duplex T7/I9.

From Figure S14C, the formation of the AND gate can be observed in lane 9. The activation of DNAzyme Z6 can only be observed with the additions of both strand I9 and I10 at the same time (lane 12), while additions of any one of them cannot lead to the activate DNAzyme Z6 (lanes 10 and 11). The results show that the slight variation of the hairpin domain has little impact on the construction of the gate, which indicates the stability of allosteric regulation of DNAzyme.

S2.4: Two-level cascading circuit

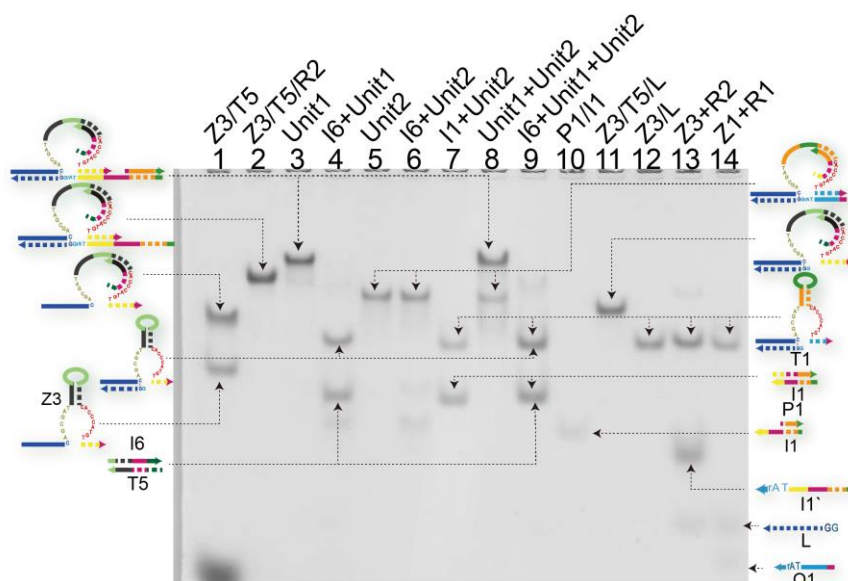Corresponding to Figure 3B, the whole PAGE analysis is shown in Figure S15.

Figure S15. Whole native PAGE analysis of two-level cascading circuit. Lane 1, products of DNAzyme Z3 inhibited by T5 ([Z3]:[T5]=2:1); lane 2, immediate product in development of Unit1 Z3/T5/R2; lane 3, Unit1 complex; lane 4, products of Unit1 triggered by I6; lane 5, Unit2 complex; lane 6, products of Unit2 in presence of input I6; lane 7, products of Unit2 triggered by input I1; lane 8, mixture of Unit1 complex and Unit2 complex; lane 9, products of two-level cascading circuit consisting of Unit1 and Unit2 triggered by input I6; lane 10, duplex P1/I1`; lane 11, DNAzyme complex Z3/T5/L; lane 12, DNAzyme complex Z3/L; lane 13, products of DNAzyme digestion ([Z3]:[R2]=1:3); lane 14, products of DNAzyme digestion ([Z1]:[R1]=1:2).

S2.5: Feedback logic circuit

Corresponding to Figure 5B, the whole PAGE analysis is shown in Figure S16.
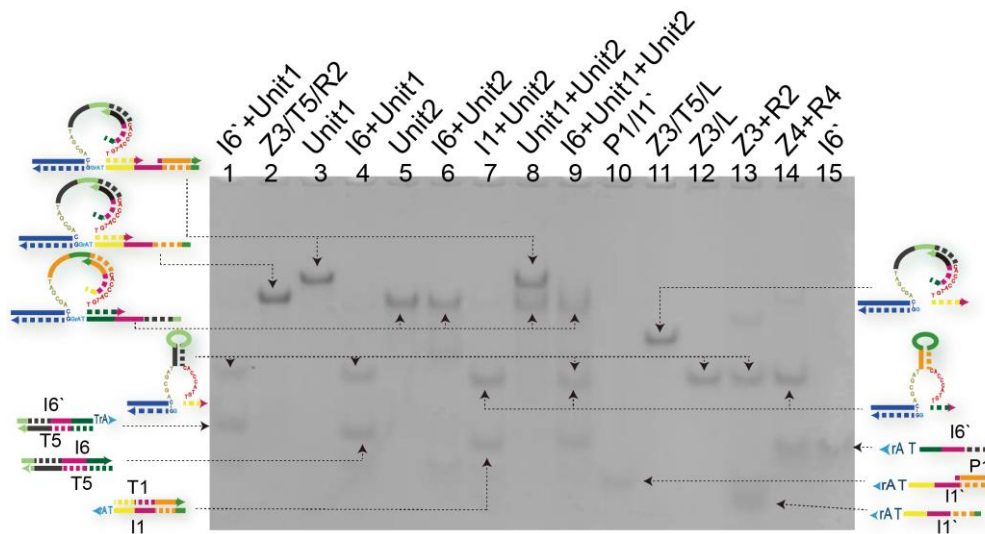
Figure S16. Whole native PAGE analysis of feedback circuit. Lane 1, products of Unit1 triggered by input I6`; lane 2, immediate product Z3/T5/R2 in development of Unit1; lane 3, Unit1 complex; lane 4, products of Unit1 triggered by input I6; lane 5, Unit2 complex; lane 6, products of Unit2 in the presence of input I6; lane 7, products of Unit2 triggered by input I1; lane 8, mixture of Unit1 complex and Unit2 complex; lane 9, products of feedback circuit consisting of Unit1 and Unit2 triggered by input I6; lane 10, duplex P1/I1`; lane 11, DNAzyme complex Z3/T5/L; lane 12, DNAzyme complex Z3/L; lane 13, products of DNAzyme digestion ([Z3]:[R2]=[1]:[3]); lane 14, products of DNAzyme digestion ([Z4]:[R4]=[1]:[3]); lane 15, strand I6`.

It is worth pointing out that the strand I6` possibly has the pseudoknots due to the RNA base rA (compare gel band in lane 10 with the one in lane 15). However, the possible pseudoknots do not hinder the DNAzyme cutting the substrate (lane 13) and the Unit 1 can also be triggered normally by the strand I6` (lanes 1 and 9).

S3: System simulation

In the following sections the braces {} are used to denote fluorescent value of reactants and the superscript Ini represents the initial concentration of reactants.

Firstly, all reaction formulas are mathematically modelled based on the explicit state-space forms (7) in a uniform schema. Secondly, experimental data were used to estimate the unknown parameters in the mathematical model based on nonlinear grey-box model (8). Finally, based on mathematical model, the reaction process was simulated using

updated parameters.

S3.1 YES gate

The YES logic operation is described through the following reaction formula,
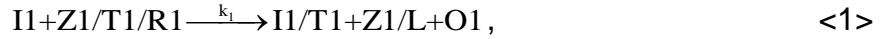
$$I1+Z1/T1/R1 \xrightarrow{k_1} I1/T1+Z1/L+O1 , \tag{<1>}$$

where k_1 is the reaction rate constant. The reaction is modeled as follows.

State equation:

$$\frac{d[O1]}{dt} = k_1 [I1][Z1/T1/R1]$$
$$= k_1([I1]^{Ini}-[O1])([Z1/T1/R1]^{Ini}-[O1]) \tag{<2>}$$

Output equation:

$$y = \{ O1 . \tag{<3>}$$

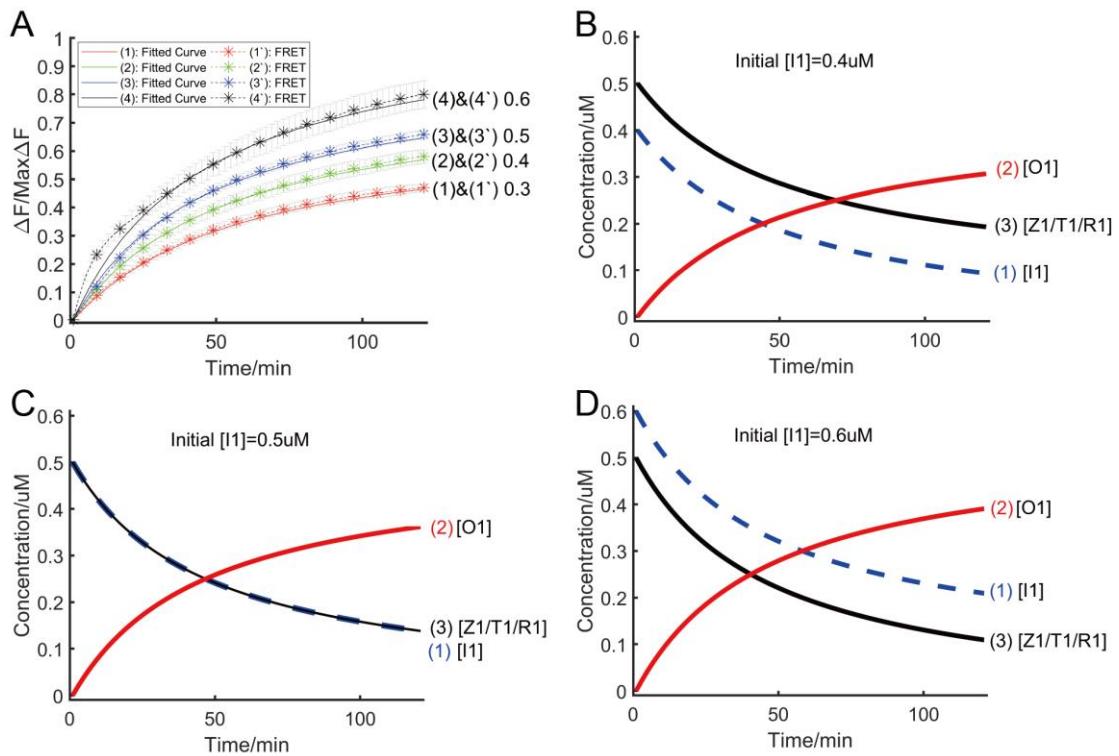The simulation results are shown in Figure S17 where k_1 =0.0013L/mol·s.

Figure S17. (A) Curve-fitting results compared to the experimental results at different levels of input concentrations of I1 as 0.3μM, 0.4μM, 0.5μM and 0.6μM, respectively. All experimental data represent the average of three replicates. Error bars represent one standard deviation from triplicate analyses. (B)-(D) Time-dependent changes of concentration of reactants, input I1, YES gate Z1/T1/R1 and output O1, at

different levels of initial input concentrations of I1 as 0.4μM, 0.5μM and 0.6μM, respectively.

From Figure S17A, the simulation results (curves 1-4) fit well with the experimental results (curves 1`-4`). As shown in Figure S17B-S17D, in the reaction process, [I1] (curves 1) and [Z1/T1/R1] (curves 3) decreased accompanying with the increase of output [O1] (curves 2), which showed that the consumptions of input strand I1 and logic gate Z1/T1/R1 were transformed to the response of gate through DNAzyme allosteric regulation. Moreover, the input-output transformation rate is dependent on the initial input concentration: higher initial input concentration, faster input-output transformation rate. In addition, according to the evolution of [I1] and [Z1/T1/T1], the process of the YES logic operation did not reach its equilibrium state during the 2-hour reaction time.

S3.2 OR gate

Corresponding to three input cases, the OR logic operations can be mathematically modelled as follows.

Case 1: OR logic operation triggered by the input strand I2 is described through the following reaction formula,

$$I2+Z1/T2/R1 \xrightarrow{k_{10}} I2/T2+Z1/L+O1 , \qquad <4>$$

$$I2/T2+Z1/L \xrightarrow{k_{11}} Z1/T2/L+I2 , \qquad <5>$$
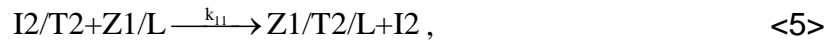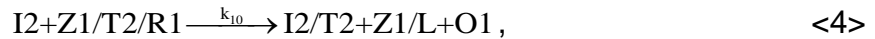
where k_{10} and k_{11} are the reaction rate constant. Without considering the time delay, the reaction is modeled as follows.
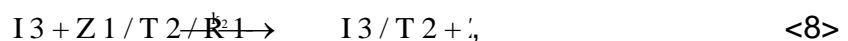
State equation:

$$\frac{d[O1]}{dt} = k_1 [I2][Z1/T2/R1]$$
$$= k_1[I2]^{In}([Z1/T2/R1]^{In}-[O1]) \qquad <6>$$

Output equation:

$$y = \{ O1 . \qquad <7>$$

Case 2: OR logic operation triggered by Input I3 is described through the following reaction formula,

$$I3 + Z1/T2/R1 \xrightarrow{k_2} I3/T2 + , \qquad <8>$$

21

where k_2 is the reaction rate constant. The reaction is modeled as follows.

State equation:

$$\frac{d[O1]}{dt}=k_2[I3][Z1/T2/R1]$$
$$=k_2([I3]^{Ini}-[O1])([Z1/T2/R1]^{Ini}-[O1])$$

<9>

Output equation:

$$y=\{O1.$$

<10>

Case 3: OR operation triggered by both inputs I2 and I3 is described through the following reaction formula,

$$I2+I3+Z1/T2/R1 \xrightarrow{k_3} I2/T2+I3/T2+Z1/L+O1,$$

<11>
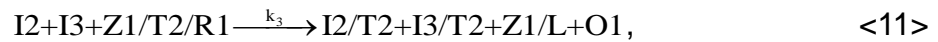
where k_3 is the reaction rate constant. The reaction is modeled as follows.

State equation:

$$\frac{d[O1]}{dt}=k_3[I2][I3][Z1/T2/R1]$$
$$=k_3([I2]^{Ini}-[O1])([I3]^{Ini}-[O1])([Z1/T2/R1]^{Ini}-[O1])$$

<12>

Output equation:

$$y=\{O1.$$

<13>

The simulation results are shown in Figure S18 where $k_1=0.00063 L/mol \cdot s$, $k_2=0.00116 L/mol \cdot s$ and $k_3=0.00221 L^2/mol^2 \cdot s$.
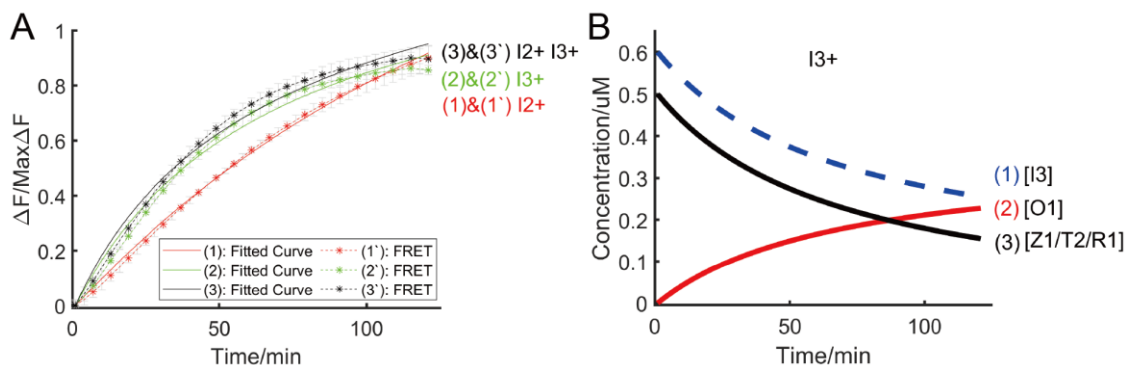

Figure S18. (A) Curve-fitting results compared to the experimental results under three input conditions. All experimental data represent the average of three replicates. Error bars represent one standard deviation from triplicate analyses. (B) Time-dependent changes of concentrations of reactants, input I3, OR gate

Z1/T2/R1 and output O1, when only I3 inputted.

For the three cases, the simulation results (curves 1-3 in Figure S18A) fit well with the experimental results (curves 1`-3` in Figure S18A) and the deviation was within the range of experimental errors. According to the reaction rate constants k_1, k_2 and k_3, the reaction of OR operation triggered by both inputs is much faster than that triggered by only single input.

S3.3 AND gate

The AND operation is described through the following reaction formula,

$$I4 + I5 + Z2/T3/\overline{T4/R}1 \xrightarrow{k_1} I4/T3 + I4/, \tag{14}$$

where k_1 is the reaction rate constant. The reaction is modeled as follows.

State equation:

$$\frac{d[O1]}{dt} = k_1 [I4][I5][Z2/T3/T4/R1]$$
$$= k_1([I4]^{Ini}-[O1])([I5]^{Ini}-[O1])([Z2/T3/T4/R1]^{Ini}-[O1]) \tag{15}$$

Output equation:

$$y = \{ O1. \tag{16}$$

The simulation results are shown in Figure S19 where k_1 =0.00116L^2/mol^2·s.
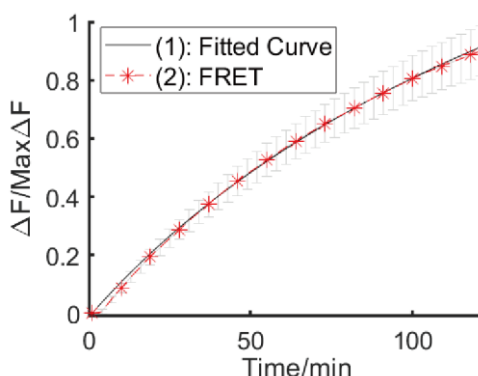

Figure S19. Curve-fitting results compared to the experimental results. All experimental data represent the average of three replicates. Error bars represent one standard deviation from triplicate analyses.

From Figure S19, the simulation result (curve 1) fit well with the experimental result (curve 2) and the deviation was within the range of experimental errors.

S3.4 Two-level cascading circuit

The process of two-level cascading circuit is described through the reaction formulas as follows,
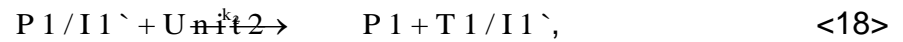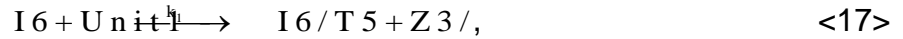
$$I6 + Unit1 \xrightarrow{k_1} I6/T5 + Z3/, \qquad <17>$$

$$P1/I1` + Unit2 \xrightarrow{k_2} P1 + T1/I1`, \qquad <18>$$

where k_1 and k_2 are the reaction rate constants. The reactions are modeled as follows.

State equation:

$$\frac{d[P1/I1`]}{dt} = k_1[I6][Unit1] - k_2[P1/I1`][Unit2]$$
$$= k_1([I6]^{Ini} - [P1/I1`] - [O1])([Unit1]^{Ini} - [P1/i1`] - [O1]) - k_2[P1/I1`]([Unit2]^{Ini} - [O1]) \quad , \quad <19>$$

$$\frac{d[O1]}{dt} = k_2[P1/I1`][Unit2]$$
$$= k_2[P1/I1`]([Unit2]^{Ini} - [O1]) \quad . \qquad <20>$$

Output equation:

$$y = \{ O1 \}. \qquad <21>$$

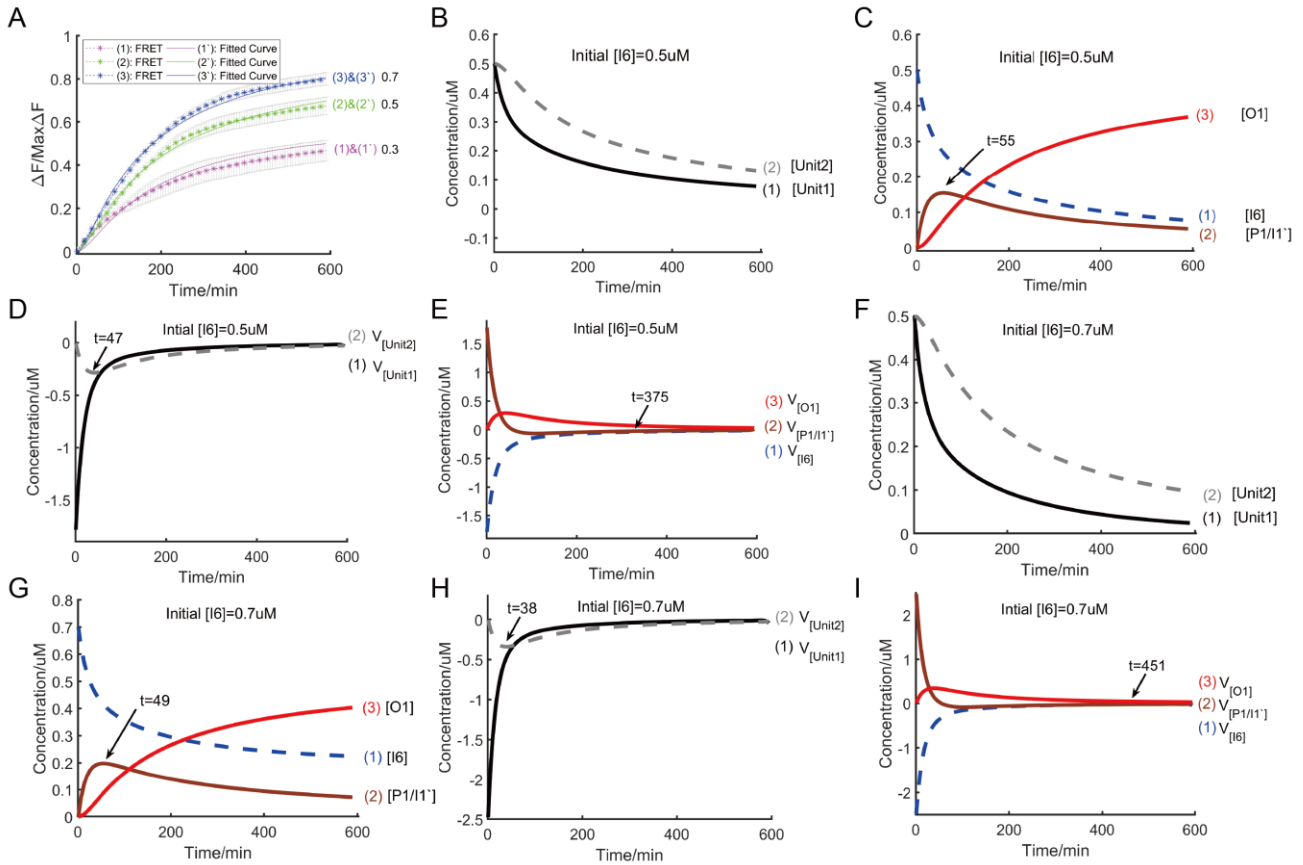The simulation results are shown in Figure S20 where $k_1 = 0.0007$ L/mol·s and $k_2 = 0.00077$ L/mol·s.

Figure S20. (A) Curve-fitting results compared to the experimental results at different levels of input concentrations of I6 as 0.3μM, 0.5μM and 0.7μM, respectively. All experimental data represent the average of three replicates. Error bars represent one standard deviation from triplicate analyses. (B)-(E) Time-dependent changes of concentrations of reactants and reaction rates in cascading process at input level I6 0.5μM. The symbol V with subscript denotes the reaction rate of reactant. (F)-(I) Time-dependent changes of concentrations and reaction rates of reactants in cascading process at input level I6 0.7μM. The symbol V with subscript denotes the reaction rate of reactant.

The simulation results (curves 1`-3`) fit well with the experimental results (curves 1-3) as shown in Figure S20A. From Figure S20B-S20I, although different initial input concentrations, the process of two-level cascading circuit presented the similar stage evolution. As marked in the figures, the time division points in different cases are different and depends on the initial input concentrations.

S3.5 Feedback circuit

Considering the protector strand P1, the trigger of Unit1 in the feedback logic circuit is

described through the following reaction formulas,
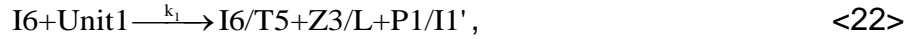
$$\text{I6+Unit1} \xrightarrow{k_1} \text{I6/T5+Z3/L+P1/I1'},$$ <22>

$$\text{P1/I1} \xrightarrow{k_2} \text{P1},$$ <23>

where k_1 and k_2 are the reaction rate constants. The reactions are modeled as follows.

State equation:

$$\frac{d[\text{P1/I1`}]}{dt} = k_1[\text{I6}][\text{Unit1}] - k_2[\text{P1/I1`}]$$

$$= k_1([\text{I6}]^{\text{Ini}} - [\text{P1/I1`}] - [\text{I1`}])([\text{Unit1}]^{\text{Ini}} - [\text{P1/I1`}] - x_2[\text{I1`}]) - k_2[\text{P1/I1`}]$$ <24>

$$\frac{d[\text{I1`}]}{dt} = k_2[\text{P1/I1`}]$$

$$= k_2([\text{P1/I1`}] - [\text{I1`}])$$ <25>

Output equation:

$$y = \{\text{P1/I1`}\} + \{\text{I1`}\}.$$ <26>

The simulation results are shown in Figure S21 where k_1=0.0016 L/mol·s, k_2=0.00002 /s when $[\text{I6}]^{\text{Ini}}$=0.05μM and 0.10μM, and k_1=0.0039 L/mol·s, k_2= 0.0001 /s when $[\text{I6}]^{\text{Ini}}$ =0.15μM.
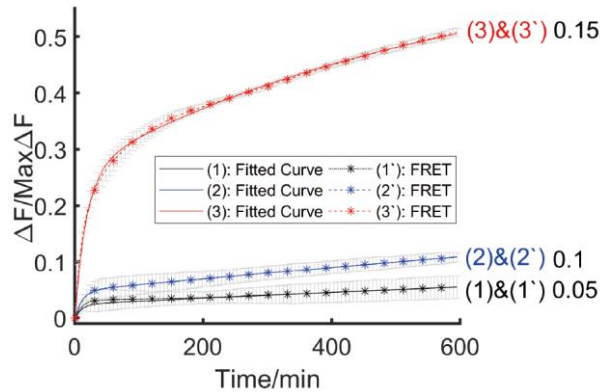

Figure S21. Curve-fitting results compared to the experimental results at different levels of input concentrations of I6 as 0.05μM, 0.1μM and 0.15μM. All experimental data represent the average of three replicates. Error bars represent one standard deviation from triplicate analyses.

The differences of reaction rate constants between the case of $[\text{I6}]^{\text{Ini}}$ =0.05μM or 0.10μM and the case of $[\text{I6}]^{\text{Ini}}$ = 0.15μM were due to the excess of inhibitor T5. When $[\text{I6}]^{\text{Ini}}$ =0.05μM or 0.10μM, the most of strand I6 hybridized with the free inhibitor T5 (approximate

0.1µM where the molar ration in preparation of Unit1 was [Z3]:[T5]:[R2]=0.5:0.6:0.5) and little of them triggered Unit1. Moreover, because there was no fluorescent signal, the hybridization between strand I6 and the free inhibitor T5 could not be detected in this experiment. So, reaction formulas <22> and <23> were just a rough description of the trigger of Unit1 in the case. On the other hand, in the case of $[I6]^{Ini}$ =0.15µM, approximate 0.05µM of the strand I6 triggered the Unit 1 and procured the rise of fluorescent signal. Based on the above analysis, it could be concluded that the Unit1 was enough sensitive to the input I6. In addition, inhibitor T5 could be used as a controller to limit the response level of the Unit1. From Figure S21, the simulation results (curves 1-3) fit well with the experimental results (curves 1`-3`).

The feedback circuit is described through the following reaction formulas,

$$I6+Unit1 \xrightarrow{k_1} I6/T5+Z3/, \qquad \qquad <27>$$

$$P1/I1`+Unit2 \xrightarrow{k_2} P1+T1/I1`+Z4/L+I6, \qquad \qquad <28>$$
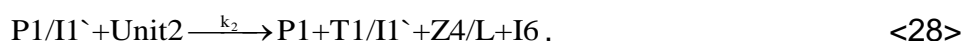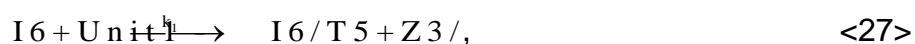
where k_1 and k_2 are the reaction rate constants. The corresponding model of the feedback circuit is as follows.

State equation:

$$\frac{d[Z3/L]}{dt}=k_1[I6][Unit1]$$
$$=k_1([I6]^{Ini}-[Z3/L]+[Z4/L])([Z3]^{Ini}-[Z3/L]), \qquad \qquad <29>$$

$$\frac{d[Z4/L]}{dt}=k_2[P1/I1`][Unit2]$$
$$=k_2([Z3/L]-[Z4/L])([Z4]^{Ini}-[Z4/L]). \qquad \qquad <30>$$

Output equation:

$$y=\{Z3/L\}. \qquad \qquad <31>$$

Because there was a one-to-one correspondence between the duplex Z3/L and the released strand I1` tagged by fluorophore, the {Z3/L} was selected as the system output variable to simplify the modelling of feedback circuit. Because of the excess of inhibitor T5 and T1, some of input I6 and the connection duplex P1/I1` could be consumed by T5 and T1 respectively, which could make some losses of fluorescent signal. Therefore, we selected

the input condition when $[I6]^{Ini}$ =0.05μM as baseline to estimate parameters k_1 and k_2 in the model. And then based on the estimated parameters k_1 and k_2, we simulated the process of feedback circuit for another two input conditions when $[I6]^{Ini}$ =0.10μM and $[I6]^{Ini}$ =0.15μM. The simulation results were shown in Figure S22 where k_1= 0.014L/mol·s, k_2 =0.00006L/mol·s.
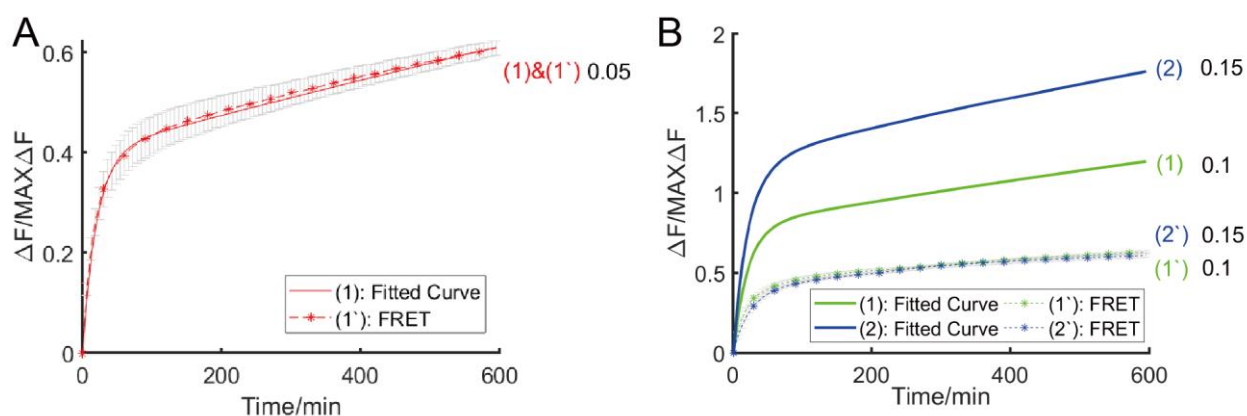

Figure S22. (A) Curve-fitting result compared to the experimental result when initial input concentration of I6 equaled 0.05μM. (B) Curve-fitting results compared to the experimental result when initial input concentration of I6 equaled 0.1μM and 0.15μM, respectively. All experimental data represent the average of three replicates. Error bars represent one standard deviation from triplicate analyses.

From Figure S22A, the simulation results (curve 1) fit well with the experimental results (curve 1`) and the deviation was within the range of the experimental errors. But in Figure S22B, the deviation was out of the range of the experimental errors. This fact was due to the excess of inhibitor T5 (approximate 0.1μM) and T1 (approximate 0.05μM where the molar ration in preparation of Unit2 was [Z4]:[T1]:[R4]=0.25:0.3:0.25) which consumed a certain number of strands I6 and duplex P1/I1`, and caused the fluorescent signals (curves 1` and 2` in Figure S22B) had almost the same final intensities in the three cases. Even so, there was a positive correlation between the fluorescence signals (curves 1` and 2` in Figure S22B) and the simulation results (curves 1 and 2 in Figure S22B).

Figure S23 and S24 shows the simulative results for the cases when the initial input concentrations were 0.1μM and 0.15μM respectively.

Similar to the case in Figure 6B, the 2-stage evolution of feedback circuit is conspicuous

as shown in Figure S23 and S24. And the oscillation can be observed through asymptotic analysis as shown in Figure S23E-S23H and Figure S24E-S24H. In addition, the terminal time of feedback depends on the initial input concentration of I6 obviously: higher initial input concentration caused the feedback circuit to reach its saturated state faster.
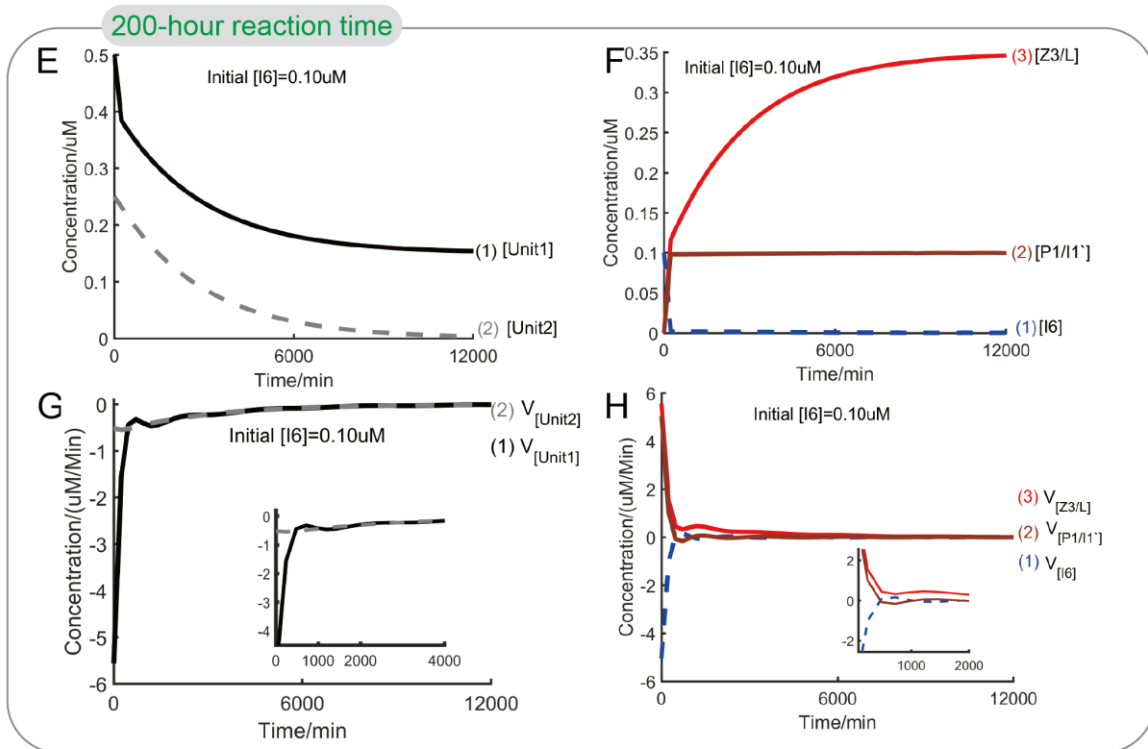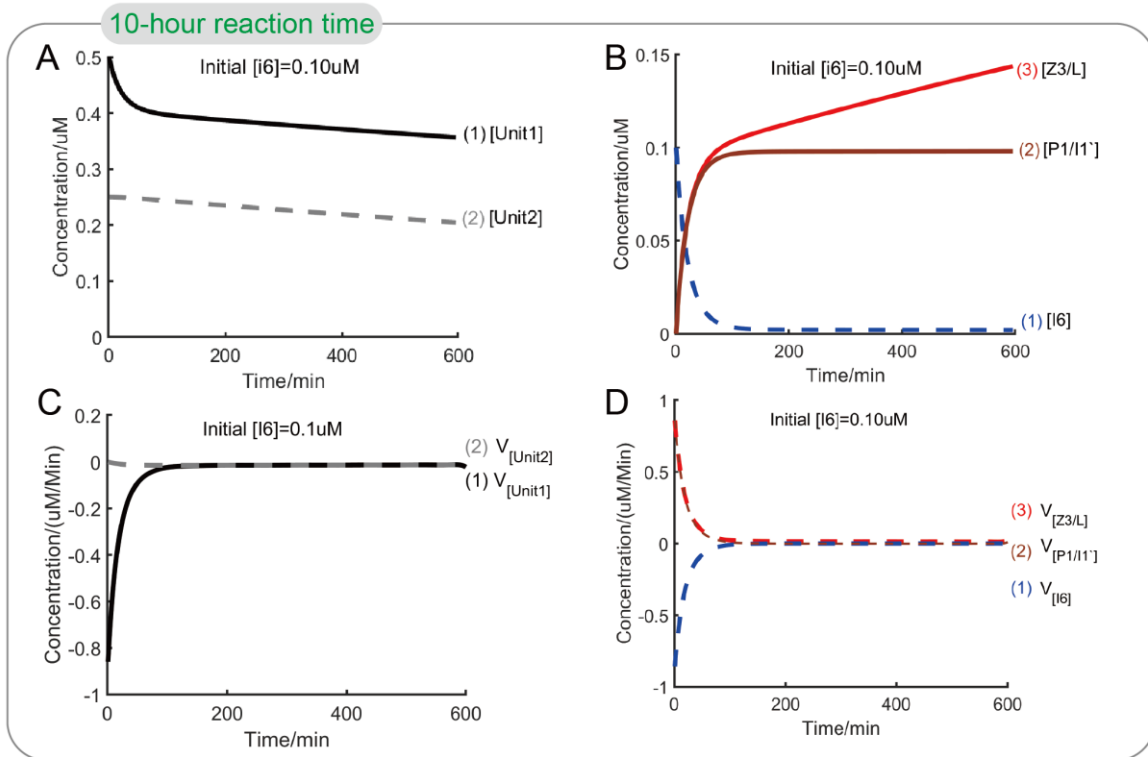
Figure S23. Simulative analysis for the case when initial input concentration of I6 equaled 0.1μM. (A)-(D) Time-dependent changes of concentrations of reactants and reaction rates in feedback circuit during 10-hour reaction time. (E)-(H) present asymptotic analysis for the feedback circuit during 200 hours of reaction time.
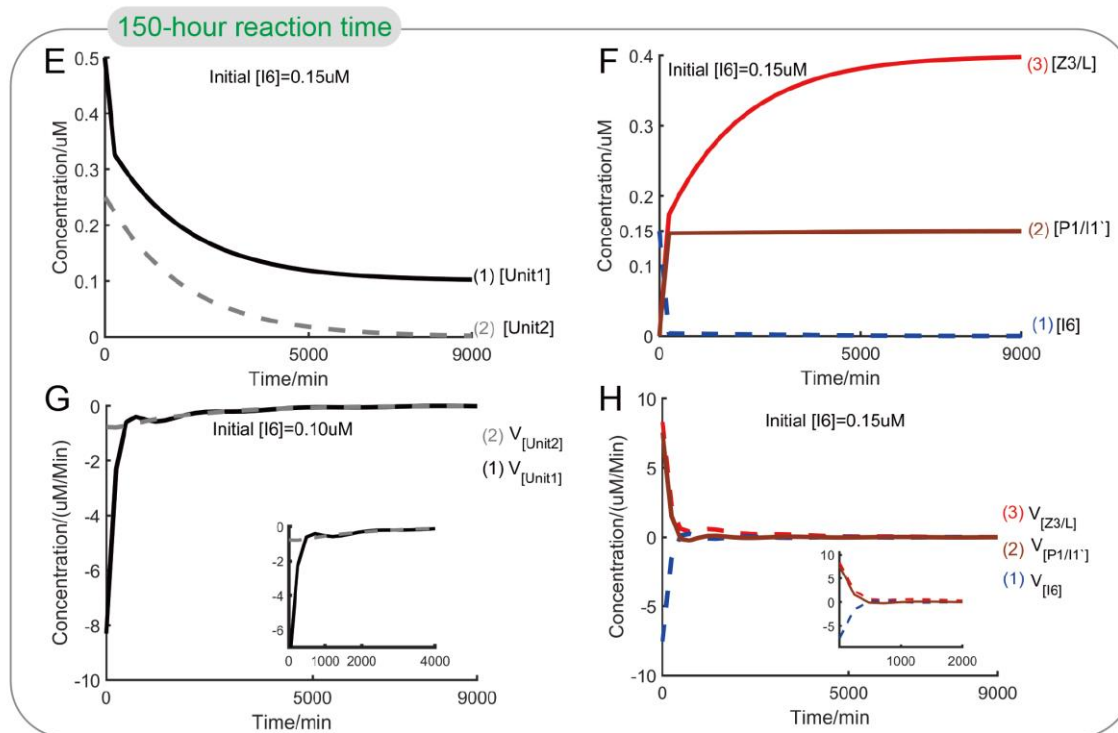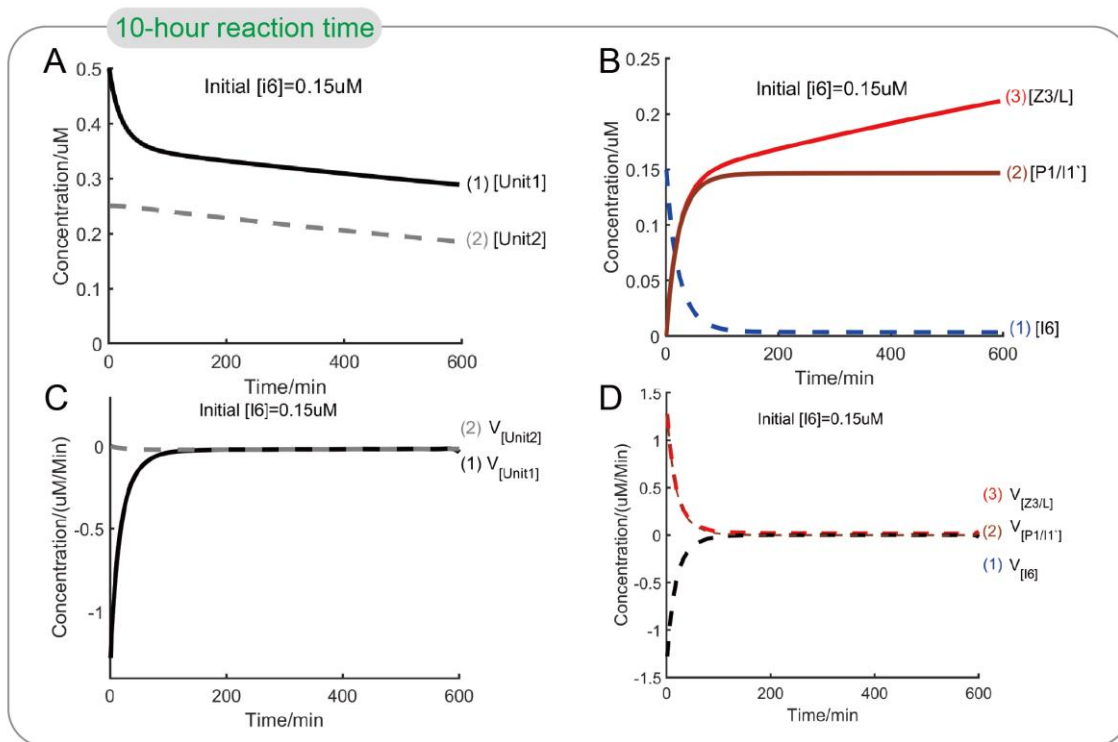
Figure S24. Simulative analysis for the case when initial input concentration of I6 equaled 0.15μM. (A)-(D) Time-dependent changes of concentrations of reactants and reaction rates in feedback circuit during 10-hour reaction time. (E)-(H) present asymptotic analysis for the feedback circuit during 150 hours of reaction time.

S4: DNA Sequences

All of the sequences used in this work were designed using Nupack (6).

Table S1.   DNA sequences.

Index	Name	Sequence (5'→3')	Length (n.t.)
1	**Z1**	TAGTGTATGTTCAGCGATACGGTACTTGTATAGTACCGTC ACCCATGTCTCTTCTC	56
2	**Z2**	TAGTGTATGTTCAGCGATACGGTACTTGTATGTGTTATCTT CTACCGTCACCCATGTCTCTTCTC	65
3	**Z3**	TAGTGTATGTTCAGCGATGACTCGTCTTGTTGACGAGTCC ACCCATGTTAACTCTC	56
4	**Z4**	TAGTGTATGTTCAGCGATACGGTACTTGTATAGTACCGTC ACCCATGTAGATATTC	56
5	**Z5**	TAGTGTATGTTCAGCGATACGGTATGTATTTGTTTACCGTC ACCCATGTCTCTTCCA	57
6	**Z6**	TAGTGTATGTTCAGCGATACGGTACTTGTATGTGTTATCTA GTACCGTCACCCATGTCTCTTCTC	65
7	**T1**	TAACTCTCATGGGTGACGGTACTAT	25
8	**T2**	CTCAATCATGGGTGACGGTACTATACAAGTCTATA	35
9	**T3**	TACAAGTACCGTATCGCTTAGCTAA	25
10	**T4**	TTCTGTTCATGGGTGACGGTAGA	23
11	**T5**	AGATATTCATGGGTGGACTCGTCAA	25
12	**T6**	CTCAATACGGTAAACAAATACATACCGTTCTATA	34
13	**T7**	CATACAAGTACCGTATCGCTTAGCTAA	27

14	T8	TTCTGTTCATGGGTGACGGTACTAG	25
15	T11	AACTCTCATGGGTGACGGTACTAT	24
16	T12	TAACTCTTCATGGGTGACGGTACTAT	26
17	T13	TAACTCTTTCATGGGTGACGGTACTAT	27
18	T10	TAACTCTCATGGGTGACGGTACTATA	26
19	T20	TAACTCTCATGGGTGACGGTACTATAC	27
20	T30	TAACTCTCATGGGTGACGGTACTATACA	28
21	I1	ATAGTACCGTCACCCATGAGAGTTA	25
22	I2	TATAGACTTGTATAGTACC	19
23	I3	TACCGTCACCCATGATTGAG	20
24	I2`	TATAGACTTGTATAGTACCGTCACCCATG	29
25	I3`	CTTGTATAGTACCGTCACCCATGATTGAG	29
26	I4	TTAGCTAAGCGATACGGTACTTGTA	25
27	I5	TCTACCGTCACCCATGAACAGAA	23
28	I6	TTGACGAGTCCACCCATGAATATCT	25
29	I7	TATAGAACGGTATGTATTTGTTTACCGT	28
30	I8	ACGGTATGTATTTGTTTACCGTATTGAG	28
31	I9	TTAGCTAAGCGATACGGTACTTGTATG	27
32	I10	CTAGTACCGTCACCCATGAACAGAA	25
33	R1	GAGAAGAGTrAGGAACATACACTA	23
34	R2	ATAGTACCGTCACCCATGAGAGTTATrAGGAACATACACTA	40
35	R3	TTCATACGAGCACCCATGAGAAGAGTrAGGAACATACACTA	40
36	R4	TTGACGAGTCCACCCATGAATATCTTrAGGAACATACACTA	40
37	I1`	ATAGTACCGTCACCCATGAGAGTTATrA	27
38	I6`	TTGACGAGTCCACCCATGAATATCTTrA	27
39	P1	GACGGTACTAT	11
40	P3	GTGACGGTACTAT	13
41	P5	GGGTGACGGTACTAT	15
42	L	GGAACATACACTA	13

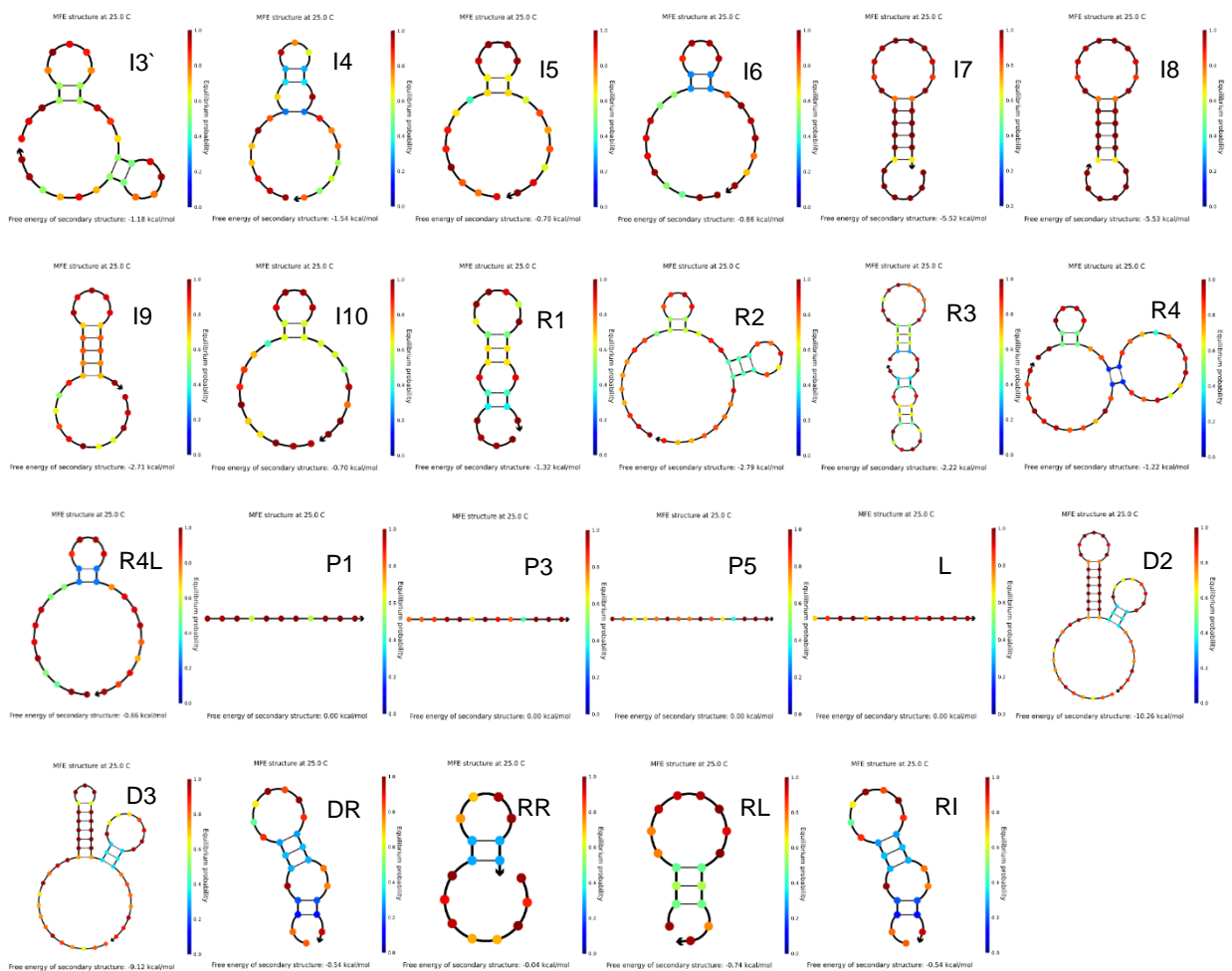| 43 | D2 | GACTCTTCAGCGATACGGTACTTGTATTTAGTACCGTCAC CCATGTTAGTGAATGTTC | 58 |
44	D3	GACTCTTCAGCGATACGGTACTATGTACCGTCACCCATGT TAGTGAATGTTC	52
45	DR	GAACATTCACTATAGGAAGAGTC	23
46	RI	GAACATTCACTATrAGGAAGAGTC	23
47	RL	GACTCTTCCTATAGTGA	17
48	RR	CCTATAGTGAATGTTC	16
49	O1	GAGAAGAGTrA	10
50	O3	TTCATACGAGCACCCATGAGAAGAGTrA	27
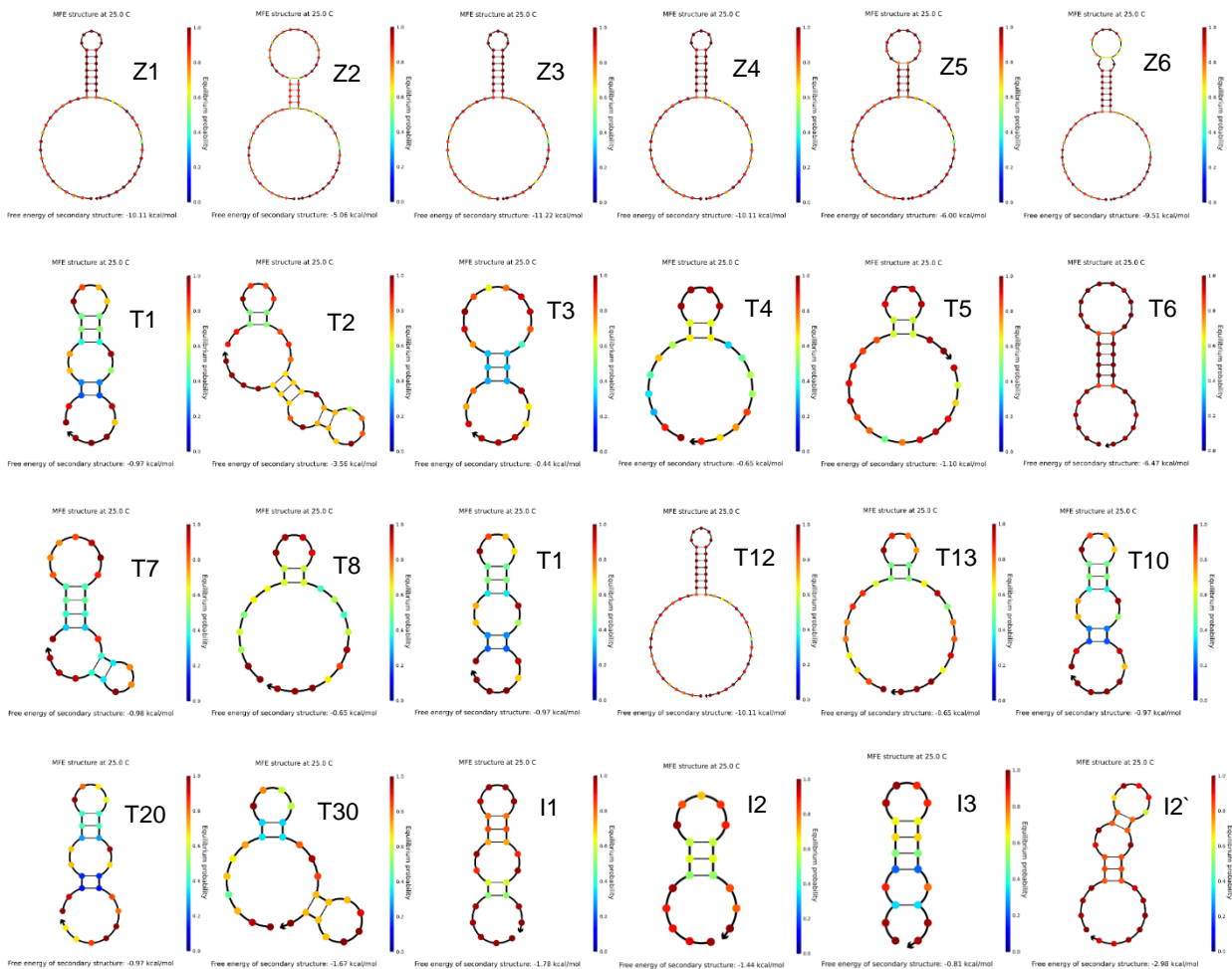
Figure S25. Nupack simulations for single-stranded sequences in Table S1.

MFE structure at 25.0 C

I10/T8

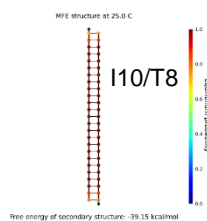Free energy of secondary structure: -39.15 kcal/mol
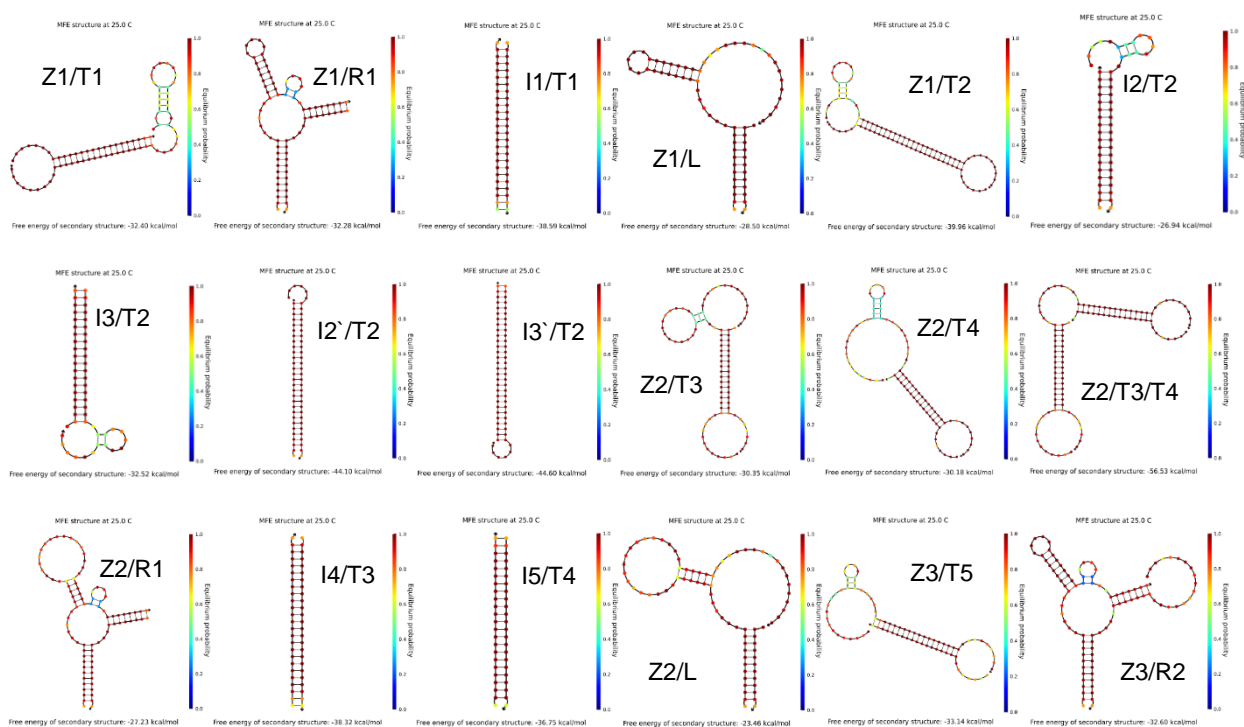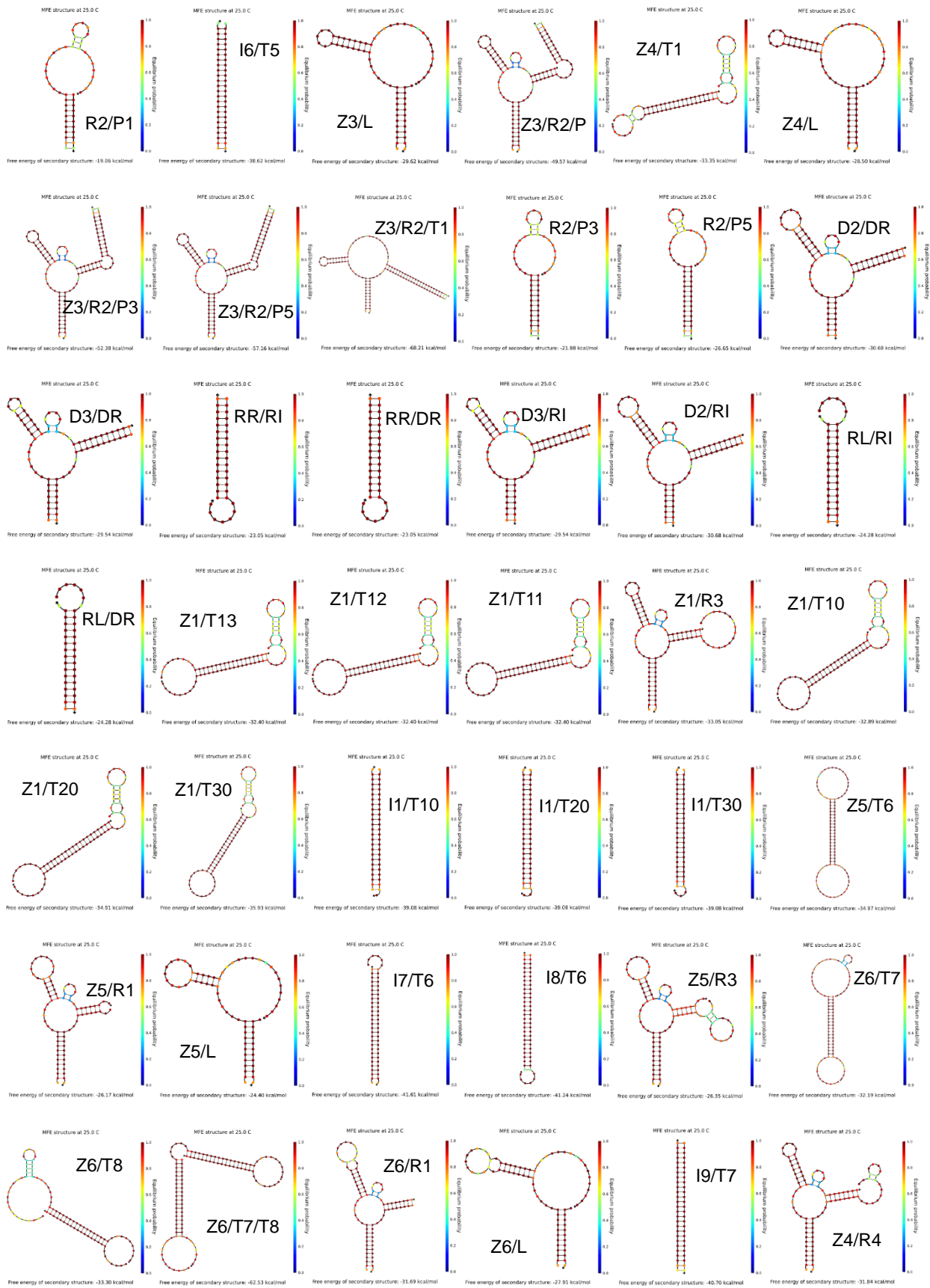
Figure S26. Nupack simulations for double-stranded structures used in YES gate, OR gate, AND gate, cascading circuit and feedback circuit.

References

1. Brown, C. W., Lakin, M. R., Horwitz, E. K., Fanning, M. L., West, H. E., Stefanovic, D. and Graves, S. W. (2014) Signal propagation in multi-layer DNAzyme cascades using structured chimeric substrates. Angew. Chem., 126, 7311-7315.

2. Brown, C. W., Lakin, M. R., Stefanovic, D., Graves, S. W. (2014) Catalytic molecular logic devices by DNAzyme displacement. Chem. Bio. Chem, 15, 950- 954.

3. Lund, K., Manzo, A. J., Dabby, N., Michelotti, N., Johnsonbuck, A., Nangreave, J., Taylor, S., Pei, R., Stojanovic, M. N., Walter, N. G., et al. (2010) Molecular robots guided by prescriptive landscapes. Nature, 465, 206-210.

4. Tian, Y., He, Y., Chen, Y., Yin, P. and Mao, C. (2005) A DNAzyme that walks processively and autonomously along a one-dimensional track. Angew. Chem., 117, 4429 -4432.

5. Genot, A. J., Zhang, D. Y., Bath, J. and Turberfield, A. J. (2011) Remote Toehold: A Mechanism for Flexible Control of DNA Hybridization Kinetics. J. Am. Chem. Soc., 133, 2177–2182.

6. Zadeh, J. N., Steenberg, C. D., Bois, J. S., Wolfe, B. R., Pierce, M. B., Khan, A. R., Dirks, R. M. and Pierce, N. A. (2014) NUPACK: analysis and design of nucleic acid systems. J. Comput. Chem., 32:170–173.

7. Norman S. N. (2014) Control Systems Engineering, 7th Edition, Wiley.

8. Bohlin, T. P. (2006). Practical Grey-box Process Identification: Theory and Applications. Springer Science & Business Media, London.